High Reliability Adhesive Joining of Metal and Composite Components

by

Barbara A. Huppe

Submitted to the Department of Aeronautics and Astronautics
in partial fulfillment of the requirements for the degree of

Master of Science in Aeronautics and Astronautics

at the

MASSACHUSETTS INSTITUTE OF TECHNOLOGY

June 2001

Author ..... Signature redacted
Department of Aeronautics and Astronautics
May 25, 2001

Certified by ..... Signature redacted
S. Mark Spearing
Esther and Harold E. Edgerton
Associate Professor of Aeronautics and Astronautics
Thesis Supervisor

Accepted by ..... Signature redacted
Wallace E. Vander Velde
Professor of Aeronautics and Astronautics
Chair, Committee on Graduate Students

High Reliability Adhesive Joining of Metal and Composite Components

by

Barbara A. Huppe

Submitted to the Department of Aeronautics and Astronautics
on May 25, 2001, in partial fulfillment of the
requirements for the degree of
Master of Science in Aeronautics and Astronautics

Abstract

In the aerospace industry, it is often necessary to join metal and composite parts. Composites are used when minimizing weight is important, and joining the materials by an adhesive layer rather than heavy metal fasteners further reduces the weight of the structure. Unfortunately, it is difficult to produce high reliability adhesive bonds between these materials due to both the differences in properties in the two materials and the strong dependence on the quality of surface preparation. It has been shown that through-thickness reinforcement, such as stitching, can increase the bond strength. Therefore, this project investigated a 3-D surface preparation method in the hope of producing higher-reliability bonds by simulating the effect of stitching. Photochemical milling was used to etch patterns into aluminum sheets. Unpatterned specimens were constructed to be a baseline or control group. Both the metal and composite surfaces of these specimens were prepared using several different methods, including sanding, anodizing, and priming. Double lap shear and double cantilever beam specimens were manufactured using aluminum and graphite/epoxy adherends. Standard FM-123 and FM-300 film adhesives were used to bond the adherends after and in conjunction with the composite cure process, respectively. Analyses were performed to take into account the effects of the thermal mismatch and of plastically deforming adherends. The results indicated that the patterning procedure is not the optimal solution in the configuration studied. Instead, simply priming the metal surfaces and sanding the pre-cured composite surfaces produced the highest strength bonds and the most consistent results.

Thesis Supervisor: S. Mark Spearing
Title: Esther and Harold E. Edgerton
Associate Professor of Aeronautics and Astronautics

Acknowledgments

I couldn't have finished this thesis without the help and support of several people. I would like to especially thank my advisor, Professor Mark Spearing, for all his help and guidance over the past five years. Many thanks also to Will McFarland for his guidance and encouragement and to Draper Labs for their financial support under contract number DL-H-526709. A special thank-you goes out to John Kane and Don Weiner for all their help in the lab and the machine shop. I would also like to thank the students in TELAC, who have all helped me technically and emotionally over the last few years. Thanks especially to Dennis for being a great UROP mentor and friend. To my UROPs Brian and Michelle, thanks for all your help and patience! To my fiance Jonathan, thank you for always being there for me when I needed it most. Finally, I would like to thank Mom, Dad, and Kimi for putting up with me all these years and for supporting and encouraging me every step of the way.

Contents

List of Figures

List of Tables

Chapter 1

Introduction

1.1 Motivation

The first aircraft ever built were constructed with wooden sections that were adhesively bonded. When metal replaced these wooden structures, mechanical fasteners were generally used instead of adhesives. Adhesive bonding processes in *metal* primary aircraft fuselage and wing structures began to be used about 50 years ago [1]. The Comet aircraft, which first flew in 1951, contained several metal joints bonded with Redux 775 adhesive. Figure 1-1 shows the adhesively bonded areas on the Comet. Forensic studies showed that there was little or no loss of strength or durability during its 30 year life.

In aircraft, adhesives are mainly used for attaching stringers to fuselage and wing skins for stiffening purposes [1]. They are also sometimes used to make metal honeycomb bonded structures for control structures such as ailerons and spoilers.

Advanced composite materials are being used more frequently in aircraft structures [2]. The first flight-worthy advanced composite component was the F-111 horizontal stabilizer. Composite stabilizers were later manufactured for the F-14, F-15, and F-16 aircraft. Boeing's 767 airplane currently uses composite materials in its floor beams and all of its control surfaces, and the 777 uses composite materials even more extensively.

Many aircraft structures therefore contain both metal and composite parts. Con-

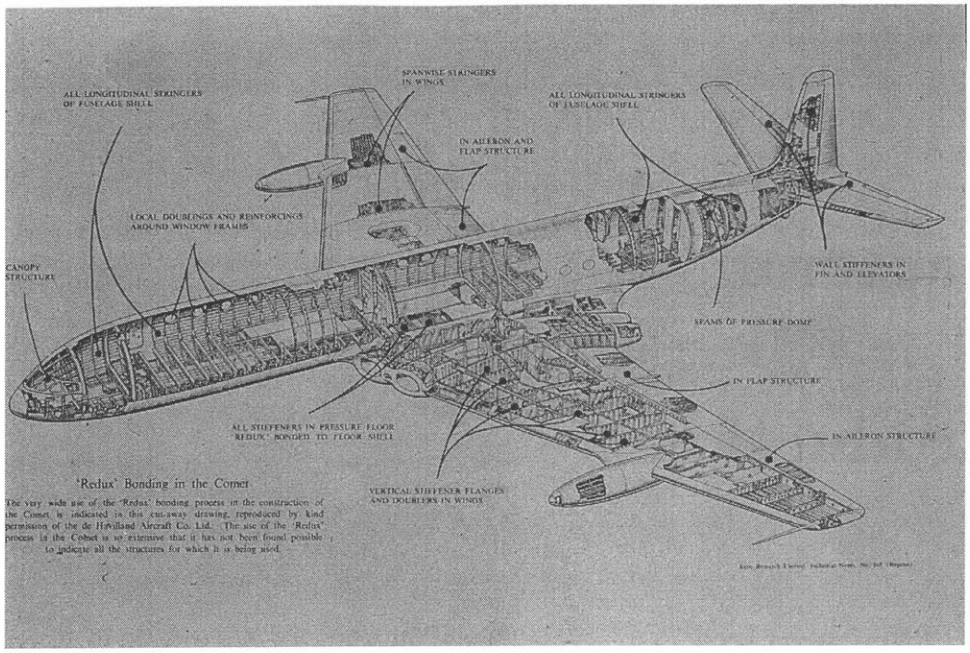

Figure 1-1: Redux 775 adhesive bonding in the comet aircraft

sequently, there is a need to join composite parts to metal ones reliably. Unfortunately, this is not as simple as it may appear. Metal structures have traditionally been joined either using metal fasteners such as rivets or bolts, or through welding processes. Composite parts, on the other hand, are often bonded together using adhesives.

Joining metals to composites therefore presents some difficulties. It is undesirable to use metal fasteners in these joints because drilling holes in the composite parts causes stress concentrations that increase the likelihood of cracking. Fasteners also add weight to the structure, defeating the purpose of using the lightweight composites. In fact, bonding can reduce the weight of a structure by 10% to 25%, depending on the type of loading [3]. Another advantage of bonding is the stiffness increase resulting from a larger contact area as compared to the spot contact of a rivet. Hart-Smith [4] states that a bonded load path is an order of magnitude stiffer than the mechanically fastened equivalent. Bonding also increases the fatigue life of metal structures by up to 15 times because of less severe stress concentrations [3]. Fragile or brittle materials are also more readily bonded than riveted. Adhesives also provide a sealing benefit to resist corrosion and to protect dissimilar materials from reacting with each other

electro-chemically. Cost can even be reduced because the cost is not directly related to the bonded area, as it is with riveting [3].

Adhesive bonding therefore seems to be a better alternative than mechanically fastening. However, there are several difficulties with producing high reliability metal/composite adhesive joints. The thermal and elastic mismatches between the metal and composite adherends are a cause for concern. The difference in the coefficient of thermal expansion (CTE) between the two materials causes thermal residual stresses to be locked into the joint during the high temperature curing process. Bonding also does not provide any through-thickness reinforcement to the joint like mechanical fasteners do. This causes adhesive joints to be susceptible to peeling loads that can cause the adherends to delaminate. Furthermore, adhesive joint strengths are very dependent on the type of surface preparation that is performed on the adherends, and the failure strengths of these joints cannot often be predicted reliably.

Table 1.1 shows a summary of the advantages and disadvantages of both bonded and bolted composite-metal adhesive joints for aircraft applications, taken from Hoskin [5].

The WASP (Wide Area Surveillance Projectile) vehicle developed by DRAPER Laboratories in Cambridge, MA contains several metal/composite interfaces, and is the direct motivation for this work. As can be seen in Figure 1-2, most of the WASP body is composite, but the fuselage connectors and wing/body connectors are all made of aluminum. The structural requirements for this aircraft are quite severe; it is launched from a cannon and must sustain very high g-loads, but the structure must also be quite light. Producing reliable metal/composite adhesive bonds is therefore critical for this aircraft.

Adhesively bonded joints can take many forms. They can be configured to take tensile, shear, peeling, or torsional stresses. In aircraft applications, adhesives are generally used to bond thin sheets of material together. Therefore, shear loading is most appropriate for these situations. One of the more common types of shear-loaded joints is the "single-lap shear" joint, shown in Figure 1-3. Unfortunately, the unsymmetric nature of this joint causes peeling loads to combine with the shear loads,

Advantages	Disadvantages
Bonded Joints	
No stress concentrations	Limits to thickness that can be joined
Stiff connection	Inspection difficult
Excellent fatigue properties	Prone to environmental degradation
No fretting problems	Requires high level of process control
Sealed against corrosion	Sensitive to peel/through-thickness stresses
Smooth surface contour	Residual stresses with dissimilar adherends
Relatively light weight	Cannot be disassembled
Damage tolerant	
Bolted Joints	
Positive connection	Considerable stress concentrations
No thickness limitations	Relatively compliant connection
Simple process	Relatively poor fatigue properties
Simple inspection procedure	Hole formation damages composite
Not environmentally sensitive	Prone to fretting
Through-thickness reinforcement	Prone to corrosion
No residual stress problems	
Harder to disassemble	

Table 1.1: Comparison of bonded/bolted joints

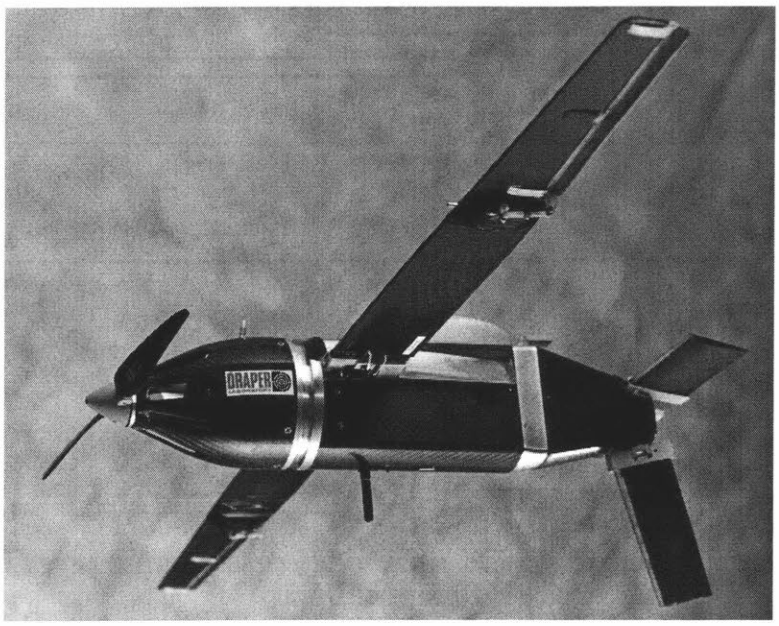

Figure 1-2: The Draper WASP aircraft

producing a more complicated stress state. Peeling loads are undesirable in adhesive joints, as previously mentioned, because there is no through-thickness reinforcement that resists these loads. Without any compressive force holding the ends of the joints together, the joints often delaminate. Figure 1-4 shows a diagram of the damage that these peeling stresses can inflict.

As discussed previously, one of the advantages of bolted joints is that the bolts or rivets provide through-thickness reinforcement to counteract any peeling loads present in the joint. Similarly, composite/composite adhesive joints are sometimes reinforced with through-thickness stitching. Stitching the ends of the composite adherends together mimics putting a compressive load on the ends of the joint. Sawyer [6] has found that just one row of stitches placed at the end of the joint can increase the static failure load by 38%. Figure 1-5 shows data from Sawyer's experiments, comparing various stitched joint configurations to the unstitched case. There is a strength improvement over the unstitched case for each of the stitch configurations.

Unfortunately, it is impossible to stitch through both composite and metal ad-

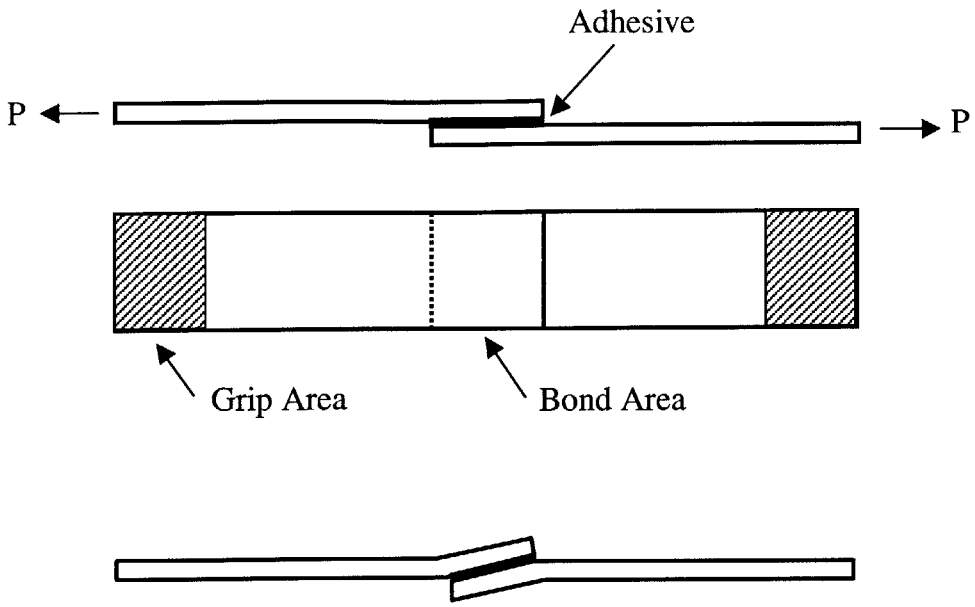

Figure 1-3: Undeformed and deformed single lap shear specimens

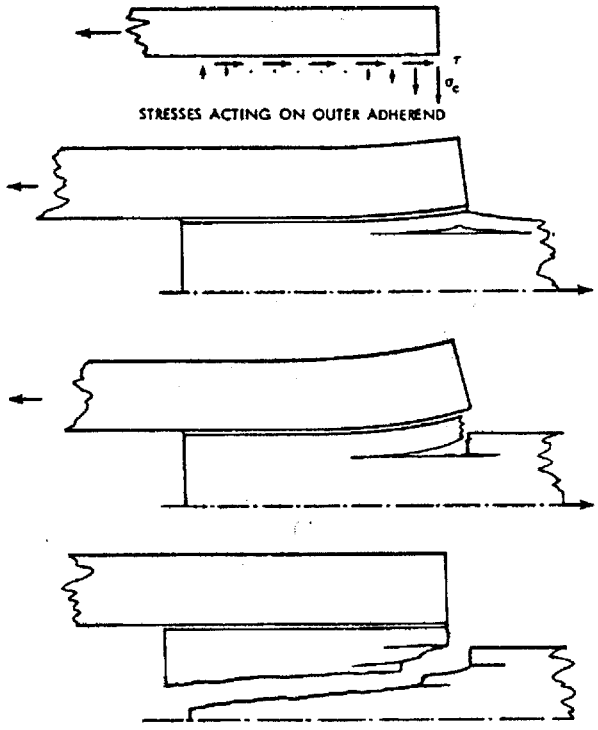

Figure 1-4: Mechanism of peel failure in a lap joint

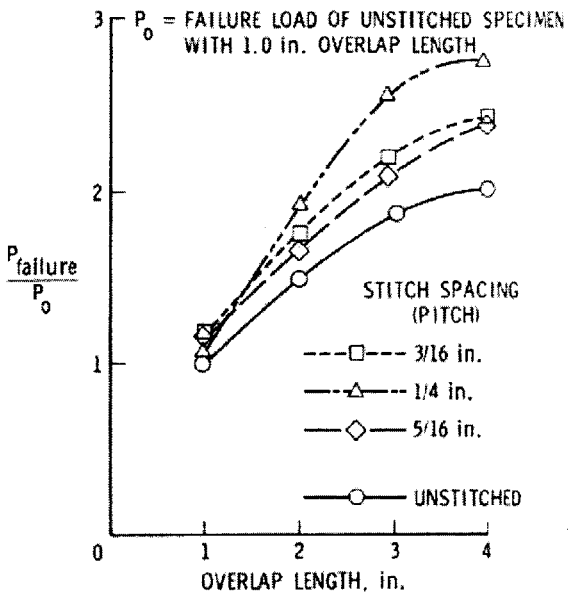

Figure 1-5: Sawyer's plot showing benefits of stitching composite lap joints

herends to provide through-thickness reinforcement to a composite/metal adhesive joint. This study investigated a novel approach to through-thickness reinforcement of metal/composite joints. Through the process of photo-chemical milling, thin grooves were etched into the metal adherend surfaces. It was hypothesized that these grooves would increase bond strength by providing a through-thickness reinforcement akin to stitching. The mechanisms motivating this hypothesis will be discussed further in Chapter 2, and experimental results will be presented in Chapter 4.

1.2 Objectives

The objective of this work is to find the best surface preparation method to produce high strength and high reliability metal/composite adhesive bonds. First, conventional surface preparation techniques, such as cleaning, sanding, etching, and priming were compared to find the best baseline procedure. Then, specimens were constructed with the innovative patterning preparation, and the test results were compared to the baseline case. Overall, it is desirable to determine the best method of preparing and manufacturing aluminum-graphite/epoxy joints in a reproduceable way.

A secondary objective is to be able to model aspects of the joint. Two important

aspects are thermal effects and plasticity effects. It is desirable to use modeling tools to be able to design a reliable joint by taking into account the thermal and plastic effects.

1.3 Thesis Outline

This thesis is divided into six chapters. After these introductory remarks, more background information will be provided in Chapter 2. The different types of adhesive joints most commonly used, thermal and stiffness mismatch issues, and information about surface preparation methods will all be discussed. Following this, Chapter 3 will then describe the manufacturing and testing details specific to this work. Chapter 4 will continue by showing the results of the mechanical testing, and Chapter 5 will discuss some of the key issues that arose during testing as well as provide some analytical and numerical modeling results. Finally, some concluding statements will be presented in Chapter 6.

Chapter 2

Background

2.1 Introduction

A review of the literature and relevant background information on several topics is presented herein. First, an overview of general adhesive joint design is presented. Following this is a discussion of the more common types of adhesive joints and the issues involved with testing them. Metal/Composite adhesive joints specifically are then discussed. The complications of thermal and elastic mismatch inherent in these bi-material joints is presented, drawing on work from prominent researchers in the field. The mechanisms for adhesive failure and the penalties incurred due to material property mismatches are discussed.

A brief discussion of the chemistry of bonding can be found in Section 2.4. Here, the importance of adequate surface preparation, as well as the mechanism of bonding, is discussed. Following this, the work of previous researchers in the field of adhesive joints is summarized. Work involving general bonding and surface preparation techniques is presented.

The mechanisms involved in "stitching" composite bonds, as well as previous research in this area, is discussed. The chapter concludes with a brief presentation of chemical milling and photoetching, the process used to create the grooved metal patterns in this work.

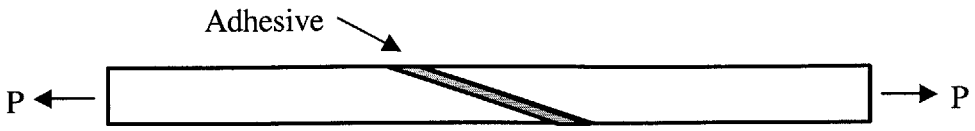

Figure 2-1: Diagram of a scarf joint

2.2 Adhesive Joints

2.2.1 Designing

Tension, compression, and shear loading situations are good candidates for adhesive bonds. However, these bonds do not perform well under peel and cleavage loading. In aircraft structures, which are predominately composed of sheet materials, tension and compression loading is impractical. Therefore, adhesive joints in aircraft are best designed for shear loading [3].

Tapered single lap joints, scarf joints, and double lap joints have higher shear strengths than single lap joints because stress concentrations are reduced in these configurations. The scarf joint (see Figure 2-1) is the most efficient because the tapering reduces stress concentrations due to shear, and it also removes the load eccentricity that causes stress concentrations due to bending. However, these joints are more costly to produce. Overall, the single lap joint provides the best compromise between cost and bond strength [3]. Single and double lap shear specimens will be discussed more thoroughly in the next section.

Bond strength is dependent on the geometry of the joint. It is directly proportional to the width of the joint and is related to the overlap length as well. More importantly, the bond strength is largely dependent on the strain in the metal at the ends of the bond. In well-designed joints, failure is initiated by the change in shape of the metal that occurs where there is a large amount of yielding [3].

The load transfer in a lap joint occurs essentially only through narrow sections at the ends of the joint. Figure 2-2 shows schematically the stress distribution in a lap joint. Reducing the overlap length causes a more even shear stress distribution in

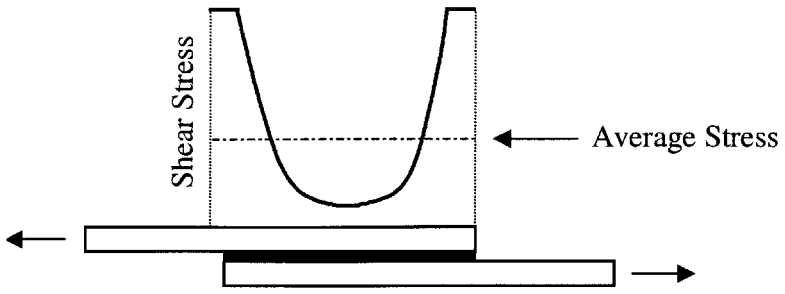

Figure 2-2: Stress distribution in a lap joint

the joint, thereby making the joint *seem* more efficient. However, attempts to save weight by reducing the overlap length and thereby better utilizing the strength of the bond should be avoided [4, 7]. Without this area of low elastic stress in the center of the joint, the peak strain at the ends of the joint would be much higher, causing the adhesive to creep and the bond to fail rapidly. The overlap length needs to be sufficiently long such that the adhesive shear stress decays towards zero in the center. This leaves a sufficiently large elastic region in the adhesive to provide resistance to adhesive creep caused by plastic deformation at the ends of the joint. Therefore, the overlap length should be designed according to the minimum stress in the center of the joint rather than the maximum stress at the ends.

In general, adhesive joints should be designed such that the strength of the bond is sufficiently greater than the strength of the adherends in that any flaw in the bond will not grow from load redistribution. If any failure occurs, it would be in the adherends. Adherend damage is easier to detect than adhesive debonding and also grows more slowly [4]. A rule of thumb is that the bonded joint should have a shear strength that is at least 50% higher than that of the adherends.

2.2.2 Testing

Past researchers have developed several test methods for adhesives and joints. Testing serves several distinct purposes: to test an adhesive batch to determine whether or not its properties have degraded with age, to compare the mechanical properties of a group of different adhesives using the same test configuration, or as in the case of this research, to determine the effectiveness of surface preparations.

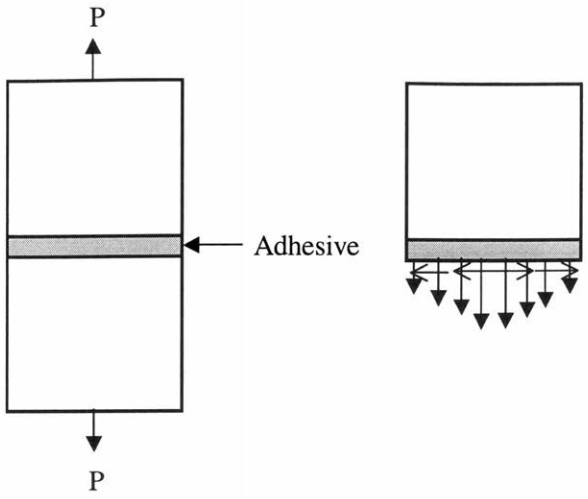

Figure 2-3: A tensile test specimen and adhesive stress distribution

Four main types of tests exist for adhesive joints: tensile, shear, peel, and fracture testing [8]. The first type, "tensile testing", is the most common type used for evaluating adhesives, although designers in general avoid loading adhesive joints in tension. An advantage of this test is that tensile modulus, strain, and strength data can be collected easily. However, researchers have found that this configuration does *not* produce a uniformly distributed stress state. Instead, shear stress is transmitted along the interface due to the differences in adhesive and adherend moduli and Poisson's ratios. Figure 2-3 shows the tensile test configuration and the resulting stress state.

The second test type is the "shear test". These tests are commonly used because the specimens are easy to construct, and they most accurately reflect the actual in-service geometry and stress state of the joint. The stress distribution in these joints is far from uniform, however. Stresses at the edges of the joint are considerably higher than those in the center of the joint. Also, the stresses in some shear test configurations can be a mixture of tensile and shear stresses. There are two main shear test configurations: single lap joints and double lap joints. While single lap joints are simpler to construct, double lap joints are often preferred because the cleavage and peel stresses are reduced due to the symmetric nature of the joints. A diagram of the single lap shear specimen was shown previously in Figure 1-3 along with its

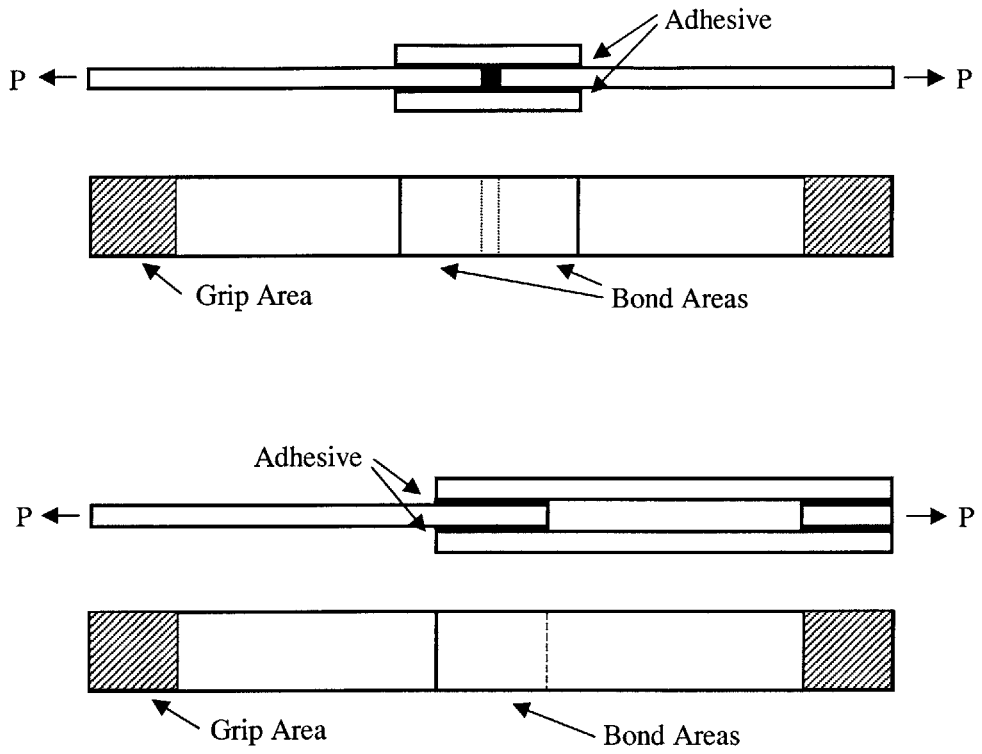

Figure 2-4: Two double lap shear configurations

deformed shape. Two different versions of a double lap shear specimen are shown in Figure 2-4. ASTM Standards D1002 [9] and D3528 [10] describe the procedures for manufacturing and testing single and double lap shear joints, respectively.

The third adhesive test type is the "peel test". These are usually used to compare different types of adhesives. The most common form is the "T-peel" test, where the ends of the specimen are bent at right angles, forming a T (see Figure 2-5). Again, the stress distribution can be rather complicated and depends on numerous factors, including specimen geometry.

The last type, "fracture testing", is the best way to obtain quantitative measures of bond strength rather than just qualitative comparisons. Shear tests are often only used to compare like specimens qualitatively, and the strength data cannot be used for design purposes without careful control and knowledge of adhesive behavior [11]. In contrast, fracture testing allows the fracture toughness of the adhesive to be directly calculated, and this can in turn be used in design. The most common geometry used for fracture testing is the Double Cantilever Beam (DCB) Test, shown

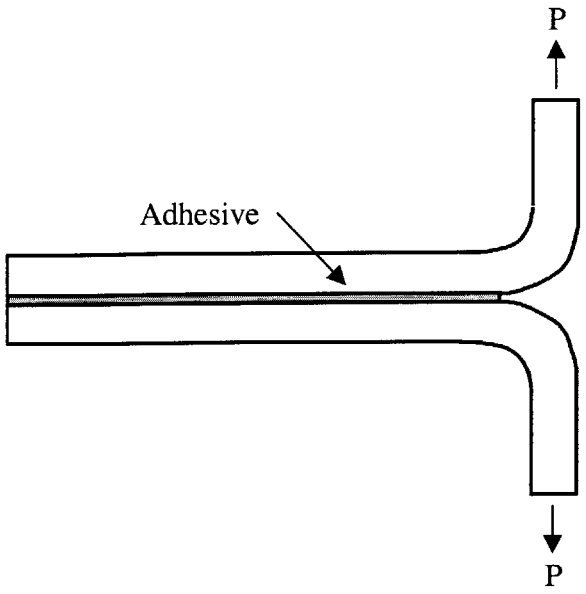

Figure 2-5: A T-peel test specimen

schematically in Figure 2-6. This test allows Mode I fracture data, including the critical strain energy release rate (fracture toughness) G_c, to be calculated. ASTM Standards D5528 [12] and D3433 [13] document procedures for performing DCB tests and calculating toughness values for composites and metals, respectively.

2.3 Metal/Composite Adhesive Joints

Joining metals to composites reliably presents challenges mainly because of the elastic and thermal mismatch between the two materials. For a given thickness, graphite/epoxy is much stiffer than aluminum. The coefficient of thermal expansion of the aluminum is much greater than that of composite. These two effects combine to produce residual stresses in the joint that cause premature failure within the adhesive.

By definition, a "balanced" joint is one where the thermal and elastic properties of the adherends are all the same. Hart-Smith [14, 15, 5] has derived theoretical solutions for the double lap joint configuration shown in Figure 2-7. Here, the adherends have the same modulus and CTE, and the total thickness of the two outer adherends is the same as the thickness of the inner one.

The mechanism for shear failure can be seen schematically in Figure 2-8. The

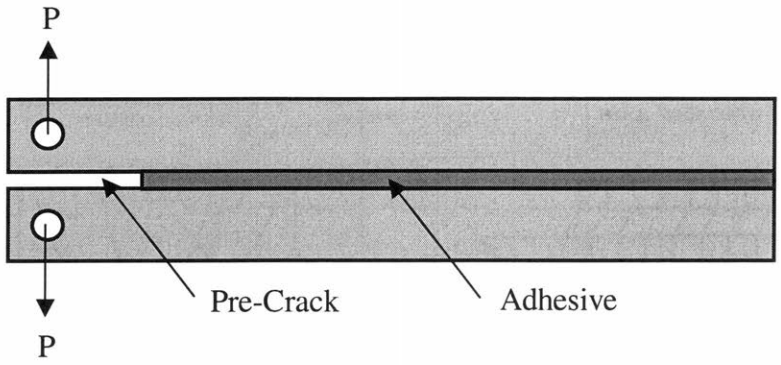

Figure 2-6: Schematic of a DCB test specimen

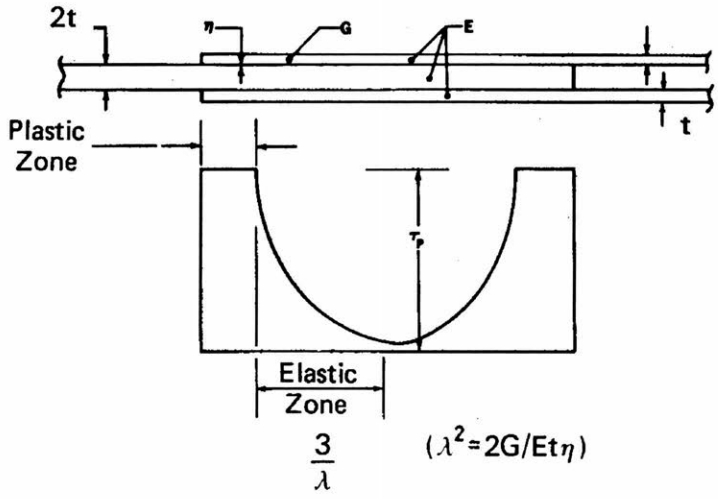

Figure 2-7: Diagram of a balanced DLS specimen used in Hart-Smith's analyses

loading is symmetric on both ends of the joint. The shear stresses and strains are concentrated at the ends of the adhesive, and this eventually causes failure.

As mentioned previously, lap shear joints are subject to peel stresses as well as shear stresses. This can cause failure, usually in the inner adherend, of a DLS joint near the edge of the overlap. This is common in cases where the inner adherend is a composite material because plies can delaminate easily.

In order to design the optimum joint and to find its maximum load carrying capability, the shear stress/strain properties of the adhesive must be known. In his calculations, Hart-Smith idealizes the actual adhesive stress/strain curve to produce

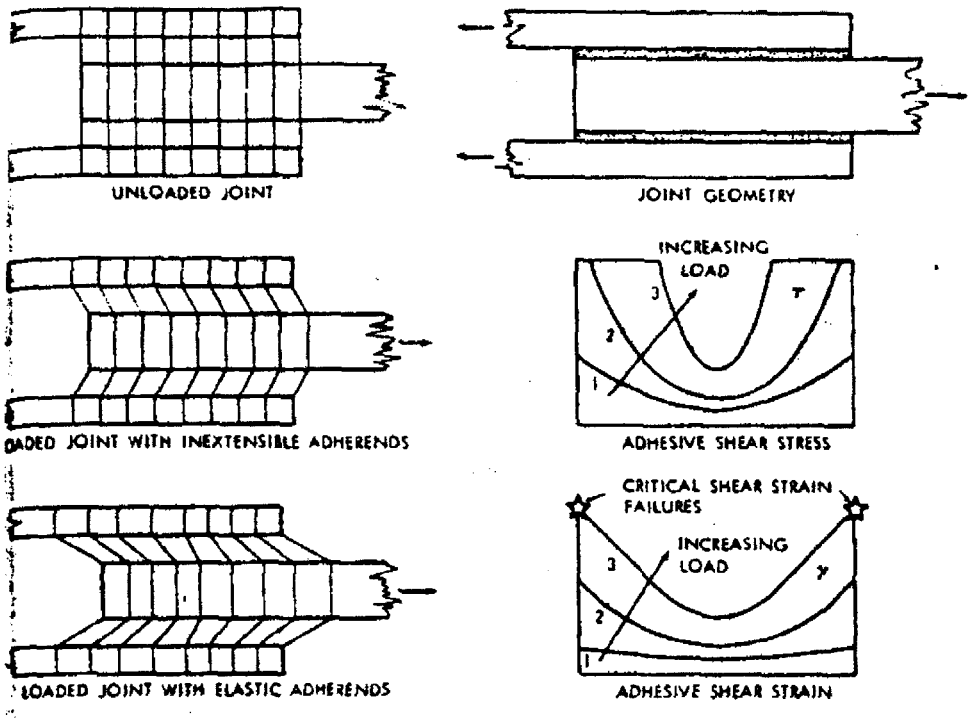

Figure 2-8: Mechanism of shear failure in a balanced DLS joint

an elastic-perfectly plastic model, as shown in Figure 2-9. The goal is to idealize the curve such that the areas underneath the idealized and actual curves are the same. Once this is accomplished, the three relevant parameters, elastic shear strain γ_e, plastic shear strain γ_p, and plastic shear stress τ_p, can be defined.

The load carrying capacity, P, of the joint is proportional to the area under the stress strain curve, and is defined as

$$P = 4\left[\eta\tau_p\left(\frac{1}{2}\gamma_e + \gamma_p\right)Et\right]^{\frac{1}{2}} \tag{2.1}$$

where E and t are the modulus and thickness of the adherends as shown in Figure 2-7, and η is the adhesive thickness. The minimum required overlap in such a balanced joint in order to obtain 100% efficiency is given by

$$l_{min} = t\frac{\sigma_{ult}}{\tau_p} + \frac{2}{\lambda} \tag{2.2}$$

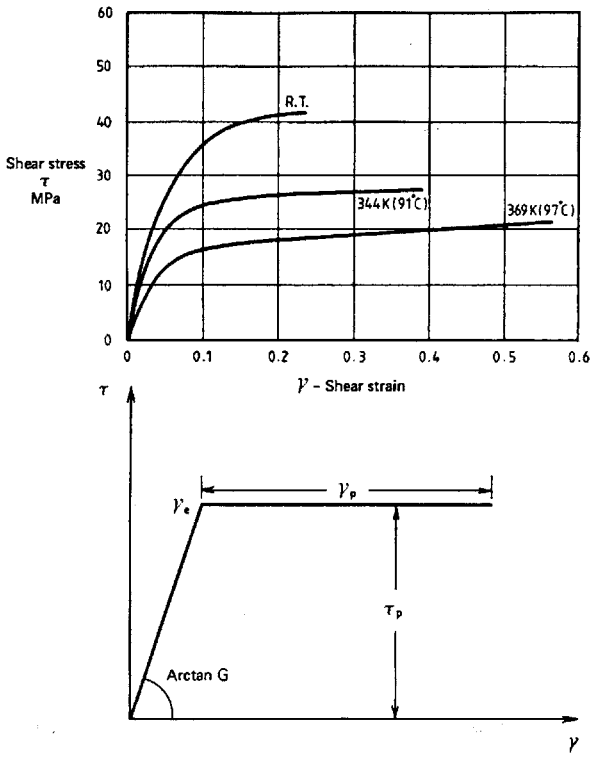

Figure 2-9: Actual and idealized adhesive stress/strain data

where λ is defined as a function of the adhesive shear modulus G and thickness η such that

$$\lambda^2 = \frac{2G}{Et\eta} \tag{2.3}$$

2.3.1 Stiffness Imbalance

In the case where the adherends have different stiffnesses, there is a reduction in the load carrying capacity of the joint. Figure 2-10 shows a schematic of a generalized double lap shear joint that allows for different adherend properties. The joint is balanced in terms of stiffness if $E_i t_i = 2E_o t_o$. If S is defined as the ratio of the stiffness of the inner adherend to the stiffness of the two outer adherends

$$S = \frac{E_i t_i}{2E_o t_o} \tag{2.4}$$

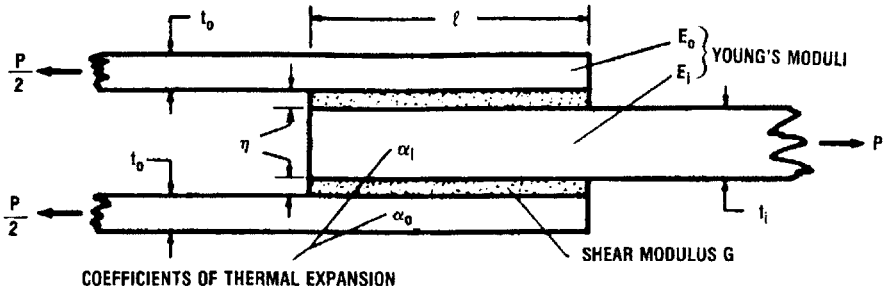

Figure 2-10: Diagram of a generic DLS specimen used in Hart-Smith's analyses

then $S = 1$ defines a balanced joint. The strength reduction factor for such a joint is dependent on the value of S and is shown below [5].

$$\sqrt{\frac{1+\frac{1}{S}}{2}} \quad \text{for} \quad S > 1 \tag{2.5}$$

$$\sqrt{\frac{S\,(1+S)}{2}} \quad \text{for} \quad S < 1 \tag{2.6}$$

The stiffness imbalance effect can be seen graphically in Figure 2-11. Here, the outer adherends are stiffer than the inner one. The load transfer is concentrated near the end of the joint adjacent to the less stiff, more extensible adherend. This causes the shear stress and strain to be much larger on that side of the joint, effectively wasting the other half of the bond.

2.3.2 Thermal Imbalance

A reduction in strength in metal/composite joints is also caused by the thermal imbalance between these two materials. Hart-Smith [5] states that in a stiffness-balanced DLS joint, the reduction in load capacity is approximately

$$2E_o t_o \Delta\alpha \Delta T \tag{2.7}$$

where $\Delta\alpha$ is the difference in CTE of the two materials and ΔT is the service temperature minus the adhesive cure temperature (or stress-free temperature). Note that

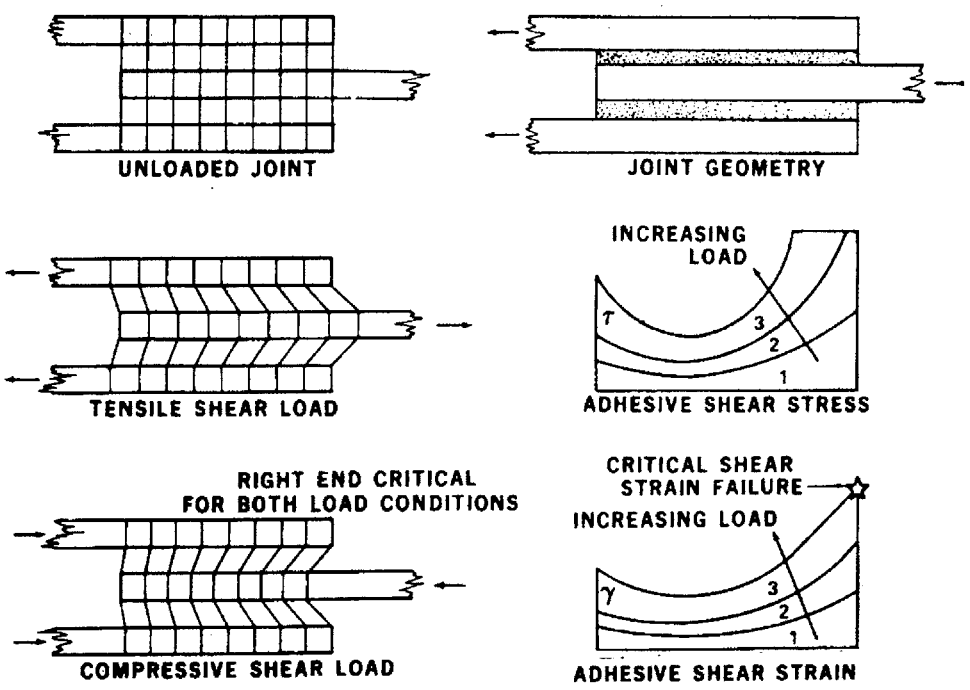

Figure 2-11: Mechanism of shear failure in a stiffness-imbalanced DLS joint

in most cases, ΔT is a negative quantity. Figure 2-12 shows the effects of thermal mismatch on a metal/composite DLS joint. Residual stresses and strains due to the temperature change cause deformation in the adhesive prior to external loading. Loading the joint in shear then causes one end of the joint to experience higher shear stresses and strains, thus accelerating failure at that end. Note that the lower two diagrams on the right of Figure 2-12 refer to tensile shear loading.

2.3.3 Combined Stiffness/Thermal Imbalance

In most practical metal/composite joints, both stiffness and thermal imbalances are present. Hart-Smith [14, 15, 5] stated that it was impossible to determine by inspection whether the adhesive near the edge of the less stiff adherend(s) or the adhesive near the edge of the stiffer adherend(s) would be more critical. This is because the effects of the thermal and stiffness mismatches could either compound each other to cause the joint to fail even earlier, or the effects could cancel each other out. There-

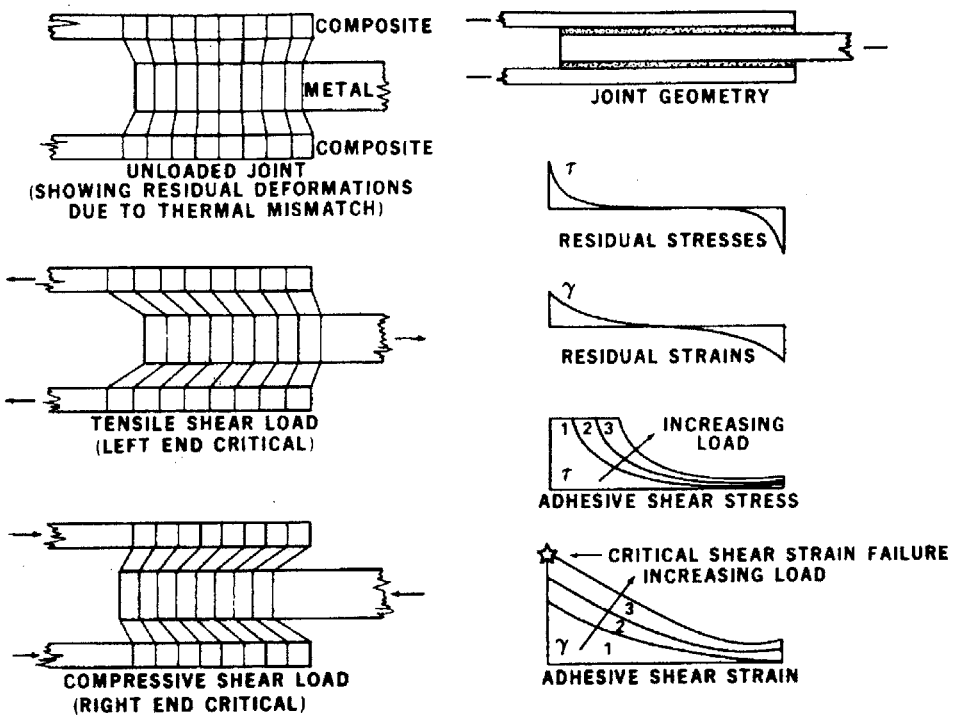

Figure 2-12: Mechanism of shear failure in a thermal-imbalanced DLS joint

fore, the strength of the joint is given by the lesser of the following two equations:

$$P = (\alpha_o - \alpha_i)\,\Delta T E_i t_i + \left[2\eta\tau_p\left(\frac{1}{2}\gamma_e + \gamma_p\right)2E_i t_i\left(1 + \frac{E_i t_i}{2E_o t_o}\right)\right]^{\frac{1}{2}} \tag{2.8}$$

$$P = (\alpha_i - \alpha_o)\,\Delta T 2E_o t_o + \left[2\eta\tau_p\left(\frac{1}{2}\gamma_e + \gamma_p\right)4E_o t_o\left(1 + \frac{2E_o t_o}{E_i t_i}\right)\right]^{\frac{1}{2}} \tag{2.9}$$

where η, τ_p, γ_e, and γ_p are the adhesive thickness, shear stress, and strain properties as defined previously. The lower of these P values would then provide an estimate for the design load of a general joint with both stiffness and thermal mismatches. A negative value of P from either equation indicates that the joint would break apart due to thermal stresses alone (without the application of mechanical loads).

2.4 Surface Chemistry

In order for a bond to be effective, chemical bonds need to form between the adherend surface atoms and the atoms within the adhesive. Davis [7] states "The basic

principles of surface preparation are that the surface must be: free of contamination, sufficiently chemically active to enable formation of chemical bonds between the adhesive and the adherends, and resistant to environmental deterioration in service, especially by hydration". Hydrated oxides that displace chemical bonds between the adherend and adhesive form on poorly cleaned metal surfaces. In general, therefore, there are three basic steps in preparing a surface for bonding [7]:

1. Degrease the surface to remove contamination.

2. Expose a fresh chemically active surface by etching or abrasion.

3. Chemically modify the surface to be resistant to hydration.

Degreasing should be performed before abrasion because solvent cleaning after abrasion can result in some partially dissolved contamination remaining on the surface. Solvents that evaporate faster are better because any unevaporated pools of solvent will spread contamination as it evaporates. Detergents should not be used because while they displace contamination from the surface, the detergent itself can then become a contaminant. It is equally important that contaminant-free wipe cloths be used in this process.

A chemically active surface can be obtained by chemically etching the material or by mechanically abrading it. Many production facilities have large chemical tanks available for etching procedures. Field facilities usually use abrading either by hand sanding with abrasive cloths or by grit blasting. Hand sanding is less desirable than grit blasting because it tends to make traps in the material that can hold contaminants or moisture. Sanding debris should be removed with a dry cloth rather than solvents. For polymer matrix composites, the recommended procedure is to use a light aluminum oxide grit blast in dry nitrogen. Ideally, this would remove the surface of the resin without exposing bare fibers.

Chemically modifying the surface can be accomplished either by anodizing or by adding a coupling agent. Anodizing produces a thin oxide film that is micro-rough and is resistant to hydration. Coupling agents are long-chain polymers that form covalent

bonds on one end with the surface oxides and hydroxides on the metal surface and that link with the adhesive on the other end during the curing process.

2.5 Previous Work

2.5.1 Metal/Composite Joints

Adhesive joints have been studied extensively, but few researchers have investigated how to improve joints between dissimilar materials. Joining dissimilar materials is difficult because of the differences in both elastic and thermal properties. The coefficient of thermal expansion (CTE) mismatch is often the cause of residual stresses being locked into the joint, and this can in turn cause the joint to fail earlier than expected.

Shetty [16] performed thermo-mechanical tests on composite-metal joints and was able to predict the trend in the critical temperature drop required to fracture the specimens. He was also able to construct failure mechanism maps showing the types of failures depending on temperature change and adherend thickness ratio.

Loftus et.al.[17] studied non-standard testing geometries for single lap composite-metal joints that were more representative of race-car type applications. They found that specimens with the composite adherend wider than the metal performed 28% better in static loading, and had fatigue lives five times longer than traditional width joints. They also found that eliminating the sharp corners in the joint increased the strength in the unequal width joints by another 23%.

2.5.2 Surface Preparations

Several studies dealing with the surface preparation of adherends have been performed. There are a few surface treatments for aluminum that have been studied extensively and are therefore widely recommended by adhesive manufacturers and ASTM standards. For example, the adhesive manufacturer Cytec suggests performing a sulfuric/chromic acid etch on the metal, followed by application of a primer to

promote adhesion.

ASTM Standard D2651 [18] documents procedures for preparing metal surfaces for bonding. For aluminum alloys, a pretreatment involving vapor degreasing, rinsing, acid/alkaline etching, and a final rinsing is recommended. In particular, acid etching solutions such as the optimized FPL etch which consists of sulphuric acid and sodium dichromate, are typically used. The FPL etching procedure is documented fully in ASTM D2651.

Researchers at The Boeing Company [19] have found that phosphoric acid anodizing is a good aluminum surface preparation. They have shown that it produces better results than the optimized FPL etch when harsh environmental conditions are present. In normal conditions, however, the FPL etch prepares the surfaces just as well as the anodizing process.

Unfortunately, the chemicals used to clean and prepare the surfaces in the recommended methods are dangerous and often carcinogenic. In response to this, researchers have developed new surface preparation techniques that use less hazardous methods. Keohan et.al. [20] developed a chromium-free cleaning procedure that involved wetsanding with a Silane solution and then priming with a proprietary anti-corrosion primer. Lap-shear and wedge test results showed that the effectiveness of this method met or exceeded that of the sulfo-chromic etch and the phosphoric acid anodizing. Blohowiak et.al. [21] performed similar tests using a sol-gel solution that was applied to etched or grit-blasted surfaces. This also resulted in bond strengths comparable to the standard anodizing methods.

Non-chemical treatments for aluminum surfaces have also been studied. Koch et.al. [22] performed tests comparing grit blasting and ion beam enhanced deposition (IBED) to traditional phosphoric acid anodizing. They found that the non-chemical treatment was a good alternative to the chemical ones.

There have also been studies on improving composite surfaces. Chin and Wightman [23] compared as-received composite specimens to using cleaner peel-ply surfaces, grit-blasting, and oxygen plasma treatments. They found that in ambient conditions, just ensuring a clean surface by leaving the peel-ply layer on the composite until just

prior to bonding gave the highest bond strength results. There was also a study on composite surface preparation by Marinelli and Lambing [24] comparing the methods of grit-blasting, corona discharging, and oxygen plasma treatments to a plain composite surface. They found that all three methods produced improvements over the as-received conditions, with grit-blasting performing the best of the three. The results varied, however, with different composite material systems.

2.5.3 Stitching

Stitching has been shown to be effective in producing high-quality composite adhesive joints. Adhesive joints have very high peel stresses near the edges of the joint, which often cause the bond to fail. Sawyer [6] discovered that by putting a transverse compressive load on the edges of these joints, the failure stress increases considerably. While this technique is not practical in most situations, similar effects can be observed if, in the case of composite joints, the ends of the joints are stitched together through the thickness of the specimen. These stitches hold the plies together, mimicking the transverse compressive load. Sawyer found an improvement of 38% in static failure load over unstitched results, when using a single row of stitches near each end of the overlap. Sawyer also noted that by improving the stitching process, fiber damage could be minimized and results could improve even further.

Glaessgen [25] performed numerical and experimental studies comparing stitched and unstitched lap joints. His experimental results showed that the stitched joints had a failure load of 2.5 times that of the unstitched joints. Entering these results into his finite element code, Glaessgen was able to model the strain energy release rate for all three modes with varying debond lengths and number of stitches, and was able to study the mechanics of load transfer in the stitches and joints.

A similar concept, called z-pinning, in which pins are inserted into the joint providing reinforcement, has been studied by Freitas [26]. In this method, ultrasonic impactors are used to insert steel pins into aluminum-to-aluminum joints. Preliminary experimental results have shown that this technique produces joints that are 2-3 times stronger than traditional bonded or bolted joints. The reason for this is

that the pins provide a smooth method of transferring load without introducing stress concentrations.

2.6 Chemical Milling

Etching has been used for centuries. Originally used to create intricate patterns in metal for artwork, it has recently been used in the aircraft industry to create complicated shapes and designs. Beginning in the 1950's, the term "chemical milling" was applied to the process of masking, scribing, and etching large metal parts to reduce the weight of a structure or to machine chemically parts that were too difficult to machine conventionally. With the advent of the computer chip and the microelectronics industry, chemical milling has seen applications on a much smaller scale. For these smaller parts, a different technique called "photochemical etching" is used. Very precise designs that are needed for computer chips can be easily and quickly produced by this method, which is analogous to the larger scale method.

The photo-etching process consists of placing a photosensitive chemical, called a photoresist, over the surface of the part. The design to be etched is then placed over the photoresist, and the whole assembly is exposed to light. This transfers the pattern onto the photoresist by exposing some parts of the resist and not others. The unexposed parts of the resist can then be washed away using a special chemical solvent, leaving the pattern on the substrate. The assembly is then placed in the etching chemical, which dissolves away the parts of the substrate that are not covered with the resist. Once the desired etching depth has been reached, the remaining resist is dissolved using a different chemical solvent, and the process is completed. This process can be seen graphically in Figure 2-13. [27]

2.7 Summary

Several researchers have therefore investigated the theory behind adhesive joints, and even metal/composite joints in particular. However, it has been shown that

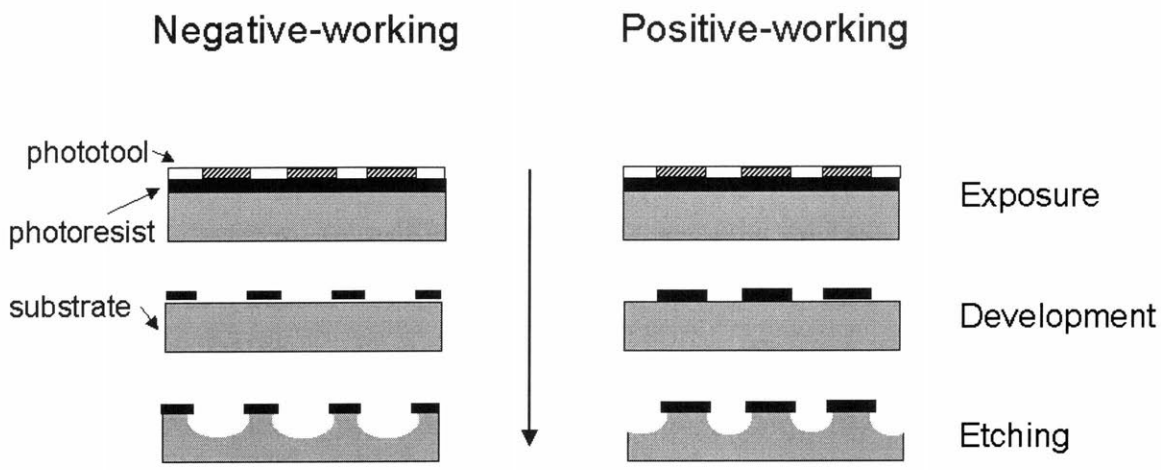

Figure 2-13: The photo-chemical etching process

surface preparation plays an important role in the strength of joints, and therefore an experimental approach is still necessary. Furthermore, a solution to the problem of reducing peeling stresses due to the lack of through-thickness reinforcement in metal/composite adhesive joints has yet to be discovered. In this work, an attempt is made to find the surface preparation method that produces the highest strength, most reliable bond.

The following chapters describe the experimental approach taken in the present study to catalogue the effects of surface preparation on two specific metal/composite joint configurations. Conventional surface preparation methods are compared with the novel metal surface patterning technique. It was hypothesized that grooves in the metal would produce a three-dimensional surface that would serve several purposes. First, the ridges in the metal act as crack barriers. Cracks propagating through the adhesive layer either have to go around the metal ridges, or the metal ridges must break in order for the crack to grow. Secondly, in a co-cured joint, the metal ridges can be made to protrude slightly into the upper plies of the composite laminate, thus providing through-thickness reinforcement to the joint. These two effects are shown schematically in the top part of Figure 2-14. Thirdly, patterns in the surface of the metal also increase the surface area that the adhesive can bond to, increasing the

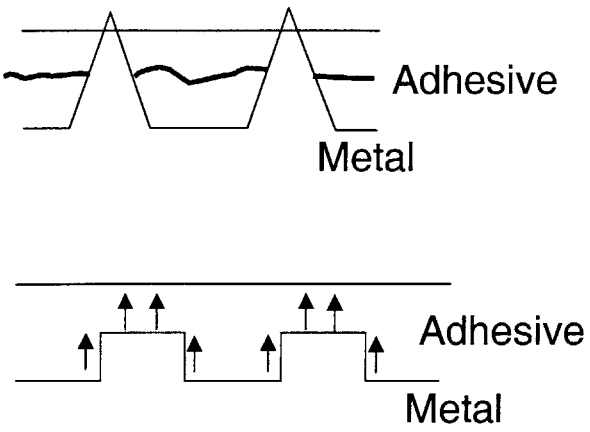

Figure 2-14: Potential strengthening mechanisms of the grooved pattern

strength of the bond. Lastly, the patterns change the stress state in the adhesive layer. In a shear test, for example, the stress is changed from pure shear to shear combined with tension. These last two effects are diagrammed in the bottom part of Figure 2-14.

These factors could all contribute to producing a better, more reliable adhesive bond between the metal and composite adherends. Chapter 3 will describe the specifics of the experimental program that was carried out in this work. The types of materials used, the joint configurations employed, the various surface preparation techniques for both the metal and composite surfaces that were used, and the specific tests that were run will all be explained. From the results of this experimental program, a recommendation as to what the optimal surface preparation method for adhesive bonding of metal to composite components will be made.

Chapter 3

Experimental Procedures

3.1 Introduction

This chapter is divided into several sections. First, a description of the types of materials used in this study, along with a summary of their relevant properties, is discussed. The two different types of joints that were manufactured in this work are described in detail. Following this are descriptions of the joint manufacturing process. The two types of curing procedures used in this study are explained, and some lessons learned from preliminary attempts are presented. Other details on how the individual specimens were cut and measured prior to testing are then discussed.

Most importantly, Section 3.3 describes the various surface preparations for both the metal and composite surfaces that were studied in this work. Section 3.4 then describes the procedures for testing both specimen configurations, and a test matrix showing all the tests that were performed concludes the chapter.

3.2 Specimen Manufacture

3.2.1 Materials

The metal used in this study was Aluminum 2024-T3. This was chosen for two reasons. First, because it is a high-strength alloy that is often used in aerospace ap-

	Aluminum 2024-T3
Young's Modulus	72.4 GPa (10,501 ksi)
Yield Stress	345 MPa (50,038 psi)
Ult. Tensile Stress	485 MPa (70,343 psi)
Poisson's Ratio	0.33
CTE	$23.2\mu m/m°C$ ($13\mu in/in°F$)

Table 3.1: Aluminum Material Properties

plications, and second, because the testing standards recommend using this particular aluminum alloy and heat treatment for adhesive bond testing. All aluminum pieces were 0.063" thick and were obtained from McMaster Supply Company.

Graphite/Epoxy of the type AS4/3501-6 manufactured by Hercules was used as the composite material in this work. This material was supplied on unidirectional rolls in pre-preg form, and was stored in a zero degree freezer until ready to use. At that point, it was thawed, unrolled, and cut into the desired sizes and ply angles. The plies were then stacked and cured at 350°F under pressure and vacuum to produce a hardened composite plate [28].

Two main adhesives were used to bond the metal and composite adherends. Both are film adhesives supplied by Cytec™, and are designated FM-123-2™and FM-300™. FM-123™cures at 225°F and was therefore used to bond already-cured composite plates to metal plates. FM-300™cures at 350°F, and can thus be used to co-cure the composite laminates and the adhesive bonds simultaneously. These two adhesives were chosen due to their curing properties and their ease of use. The film adhesive is very easy to apply, and maintains an even bond thickness during the manufacturing process.

Tables 3.1, 3.2, and 3.3 show the relevant material properties of the aluminum, composite, and adhesives.

3.2.2 Joint Types

Two different types of joints were manufactured and tested in this study: double lap shear (DLS) and double cantilever beam (DCB) specimens. DLS specimens were

	Graphite/Epoxy
Young's Modulus	148 Gpa (21,470 ksi)
Ult. Tensile Stress	1660 MPa (240,763 psi)
Poisson's Ratio	0.28
CTE	$0.02\mu m/m°C$ $(0.01\mu in/in°F)$
Cure Temperature	177°C (350°F)

Table 3.2: Graphite/Epoxy Material Properties

	FM-123-2^{TM}	FM-300^{TM}K
Shear Strength	35.5 MPa (5145 psi)	40.3 MPa (5850 psi)
Curing Temperature	107°C (225°F)	177°C (350°F)

Table 3.3: Film Adhesive Material Properties

chosen because most adhesive joints are loaded in shear, and the DLS specimen provides a symmetric alternative to the often-used single lap shear specimen. DCB tests were used to obtain a quantitative measure of the fracture properties of the bond, as well as providing durability data. General information about the qualities of these joints can be found in Section 2.2.

It was decided that sixteen-ply thick unidirectional $[0_{16}]$ graphite/epoxy laminates would be used to provide a worst-case scenario for the thermal-expansion mismatch between the metal and composite. This laminate has a CTE of approximately zero, while the aluminum's CTE is significantly higher (12.89 μin/in°F). By tailoring the composite ply angles in the laminate, a higher CTE that more closely matches the aluminum can be achieved. The unidirectional laminate used in this study has a CTE that differs the most possible from that of the aluminum. Therefore, any effects due to thermal mismatch, such as high thermal residual stresses in the joints, will be maximized by this configuration.

The dimensions of all composite and metal pieces were chosen to best match the test configurations recommended by the ASTM standards [10, 12, 13]. Figures 3-1 and 3-2 show the dimensions and configurations of the DCB and DLS specimens used in this study, respectively.

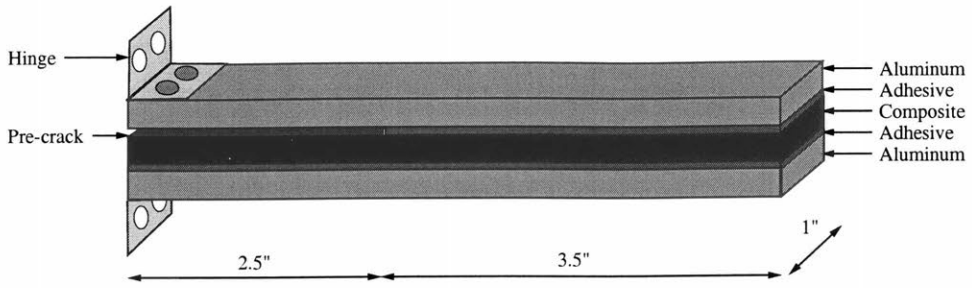

Figure 3-1: Schematic of the DCB specimens

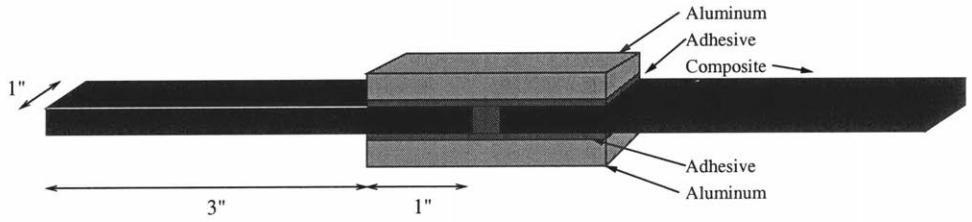

Figure 3-2: Schematic of the DLS specimens

3.2.3 Preliminary Attempts

Before a test matrix was established, a few trial runs were performed to establish a manufacturing procedure. DLS specimens were manufactured by first cutting separate metal and composite pieces, and then lining up the pieces by eye and bonding with various adhesives. All the metal pieces were first prepared by acetone wiping and sandpaper abrasion. The composite pieces were dusted with lint-free towels.

Four different adhesives were used in this first study. Because the preferred adhesive, FM-123^{TM}film adhesive manufactured by Cytec^{TM}, requires an elevated temperature cure which causes warping or residual stresses in bonds where there is a thermal expansion mismatch between the adherends, it was decided to survey three room-temperature adhesives in addition to FM-123^{TM}. FM-123^{TM}was used to bond three specimens by heating at 240°F for two hours and placing several weights on top to apply pressure. Three specimens each were bonded with West Systems 2-part epoxy #206 (12-hour cure), epoxy #205 (6-hour cure), and 5-minute epoxy. These nine specimens were aligned, bonded, and placed under a vacuum overnight to cure. They were then tested for strength as described in Section 3.4.

The following conclusions were drawn from these tests:

1. Cutting the adherends individually before bonding causes alignment difficulties
2. Room-temperature adhesives performed less well than FM-123^{TM}
3. The composite surface preparation is crucial
4. With a few modifications, this procedure should produce high quality bonds

The following sections will describe how the rest of the specimens were prepared.

3.2.4 Bonding Procedures

Two types of bonding methods were used in this work: Secondary Curing and Co-Curing. Secondary curing means that the composite laminates are cured first, alone. Then a second, separate cure is performed to cure the adhesive that bonds the metal to the cured composite plate. In co-curing, the composite plies and the adhesive are all cured together at the same time.

Secondary Cures

Secondary curing was therefore a two-step process. First the composite laminates were cured in an autoclave under high temperature, pressure, and vacuum following the standard TELAC procedure [28]. They were then post-cured in a 350°F oven for 8 hours. The edges were trimmed off using a water-cooled diamond-tipped circular saw, and the plates were cut to the sizes required for the specimens (two 4-inch wide sections for a DLS specimen and one 6-inch wide section for a DCB specimen). Next, the metal pieces were cut to size (two 2 1/8 inch pieces for a DLS specimen and two 6 inch wide pieces for a DCB specimen) using a metal shear.

If specified, both the metal and composite pieces were treated with a surface preparation. The details of this can be found in Section 3.3.

Once all the pieces were ready, film adhesive FM-123-2^{TM}was applied to one side of each metal piece. No adhesive was placed on a 2.5 inch section of one of the DCB metal pieces to allow for the pre-crack. Instead, a piece of Teflon was inserted in its place. A curing table was prepared and cork dams were placed around the

assembly so as to keep the bonding structures in place. The specimens were then assembled on the table using spacers to align the parts correctly. Teflon was placed over the specimens to keep them from sticking to the metal top plates that covered the specimens to apply even pressure during curing. The entire assembly was covered with vacuum bagging and placed in the autoclave. A diagram of the bond cure set-up for the DLS specimens can be seen in Figure 3-3. The specimens were then cured for 2 hours at 225°F at 40 psi of pressure under vacuum.

Co-Cures

For co-cures, there is only one cure instead of two. Once the composite plies were stacked to form a laminate, they were then cut to size using a sharp utility knife. Adhesive FM-300^{TM}was applied to the metal pieces as before. The specimens were assembled on the prepared curing table, once again using metal spacers and cork dams to align everything properly. This procedure is more difficult to carry out than with the secondary cure because the composite parts are very sticky and flimsy. Also, more cure materials such as bleeder paper and extra Teflon are needed because the uncured composite parts will bleed out a large amount of epoxy during the curing process. A diagram of the cure set-up for a DLS specimen plate is shown in Figure 3-4. Once the assembling process was finished, the table was placed in the autoclave and cured using the standard composite cure cycle, which involves a one hour hold at 240°F and a two hour hold at 350°F, all under 85 psi of pressure and vacuum [28].

3.2.5 Specimen Preparation

Once the specimens were cured, they were then cut into one inch wide specimens using either a diamond-tipped, water-cooled, circular saw blade or a water-jet cutter. The edges of the plates were not used to avoid the regions of epoxy and adhesive spill out. If necessary, the tops and bottoms of the specimens were also trimmed. This generally was only needed in the co-cured joints. The metal parts of the specimens were then filed to remove sharp edges and corners. All the specimens were then

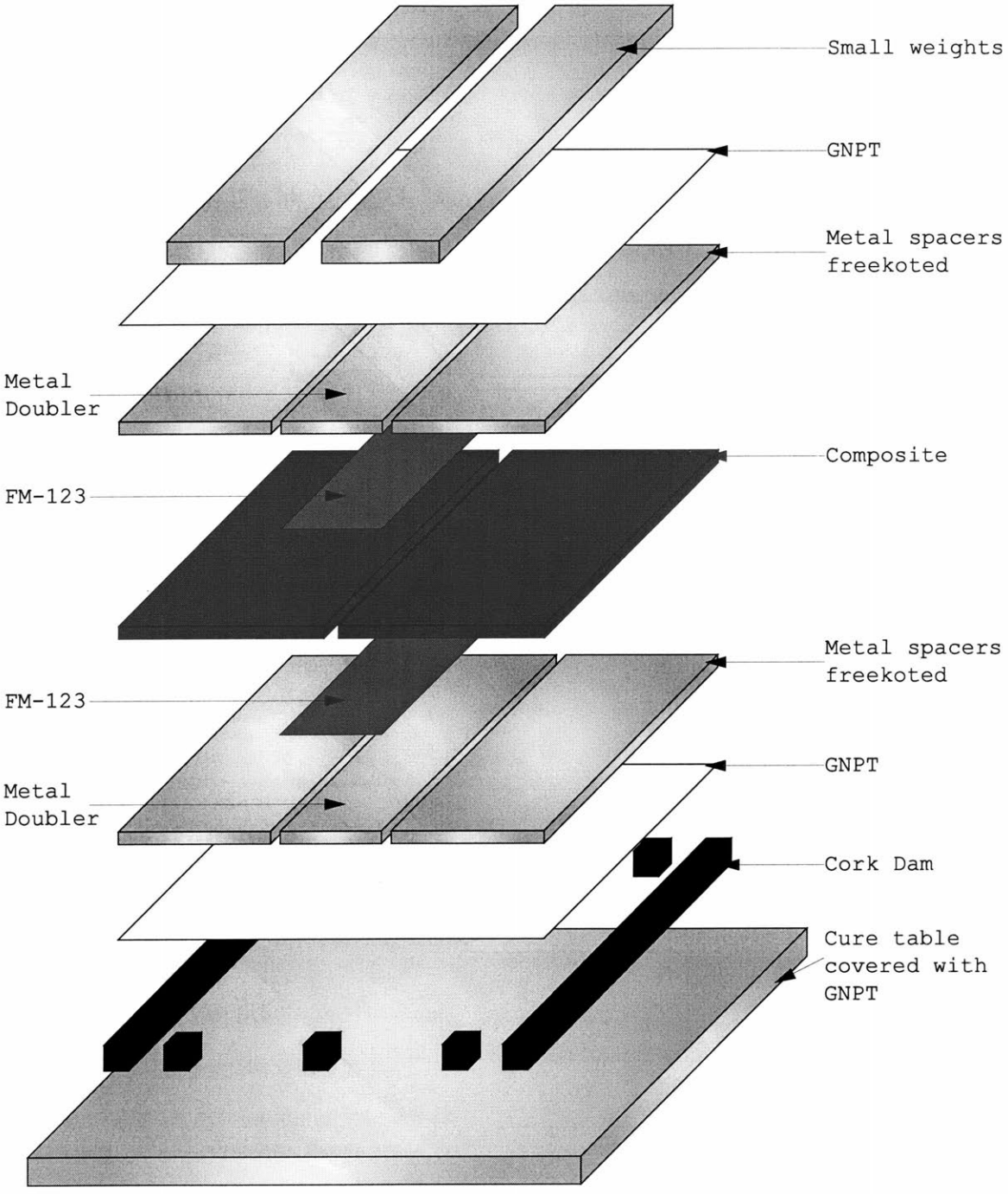

Figure 3-3: Diagram of a DLS bond cure set-up

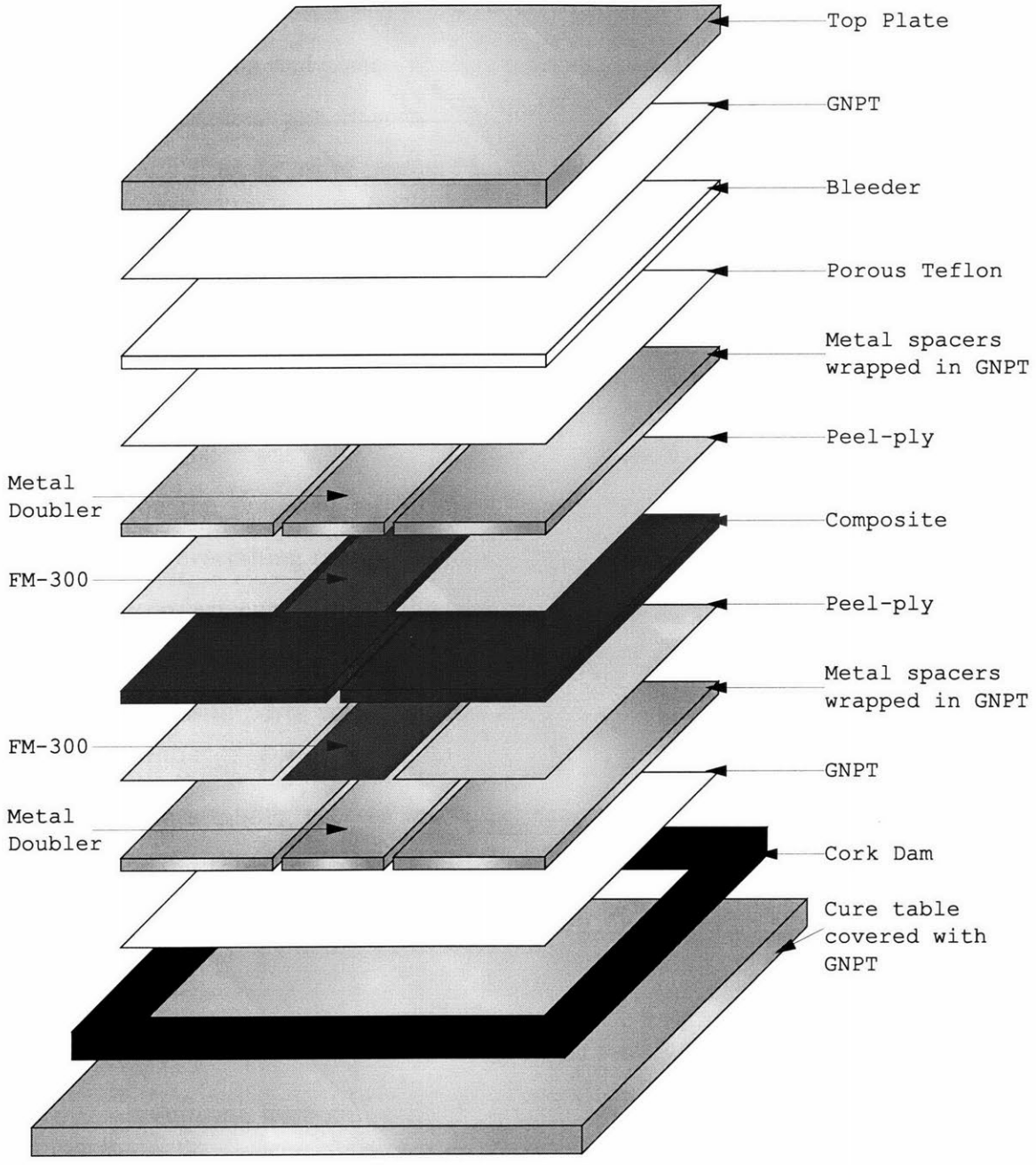

Figure 3-4: Diagram of a DLS co-cure set-up

carefully measured using calipers. Thicknesses, widths, and lengths of all bond areas were recorded, as well as the pre-crack lengths of the DCB specimens. Marks were placed on the edges of the DCB specimens at the beginning of the bonded region at 2 mm intervals up to 10 mm and 5 mm intervals from 10 mm to 30 mm.

In order to test the DCB specimens, it was necessary to bond hinges onto the ends (see Figure 3-1). This was achieved using 5-minute epoxy and 1-inch wide brass hinges supplied by the McMaster Carr Company. Both the hinges and the ends of the specimens were cleaned with acetone and roughened with 80 grit sandpaper before bonding. The hinges were left to cure at room temperature for at least 24 hours before testing began.

3.3 Surface Preparations

Several different metal and composite surface preparations were explored in this study. In most cases, the same preparations were used in both DLS and DCB specimens. Some of the surface preparation techniques were also used on both co-cured and secondarily-cured specimens. The results from the tests will be described in Chapter 4.

3.3.1 Metal Surfaces

As discussed previously, it was desired to compare bonds with etched grooves in the metal to the best baseline bonds with more conventional metal surface preparations. In this section, the different techniques that were used to prepare the metal surfaces will be described.

Sanding

Sanding was the simplest metal surface preparation used. In this method, 80-grit sandpaper was used to roughen the surfaces to be bonded. The sandpaper left scratches in the surface of the aluminum that were visible to the naked eye. The aluminum was sanded by hand until an evenly scratched surface was obtained. The

abraded surfaces were then wiped with acetone using either lint-free wipes or cheesecloth. Care was taken to avoid putting fingerprints or other contaminations on the areas to be bonded. The metal was sanded immediately before bonding to avoid oxidation of the surface prior to bonding.

Priming

Aluminum was FPL-etched and primed with Cytec's BR-127^{TM}anti-corrosion primer. The FPL (Forest Products Laboratory) etch is a common sulfuric acid and sodium dichromate etch used in pre-bonding applications. BR-127^{TM}primer is a modified epoxy phenolic classified as a general aerospace primer, and has been used in virtually every commercial aircraft built since its development. Because the metal must first be etched with hazardous chemicals before a thin layer of primer is applied, and because the tools and materials to do this were not available locally, plain aluminum was shipped to the Poly-Metal Finishing Co. in Springfield, MA for the etching and priming processes.

The primed metal was shipped wrapped in paper to keep the surfaces clean. Once again, care was taken to avoid contaminating the surface, and the metal was only removed from the paper wrappings immediately prior to bonding. No additional cleaning procedures were used before bonding.

Anodizing

Anodizing is another common means of preparing aluminum surfaces for bonding in the aerospace industry. Aluminum was sent to the Duralectra Company in Natick, MA where it was hardcoat anodized. In this process, the aluminum is put in a sulfuric acid bath where it attracts negatively charged oxygen ions in the solution. This leaves an aluminum oxide coating on the metal that is very porous and that allows the adhesive to latch on to the metal surface and produce a strong bond.

The anodized metal was once again shipped wrapped in paper to avoid oxidation and contamination. The same precautions were taken with this material as previously noted. No additional chemicals or procedures were used to clean the anodized metal

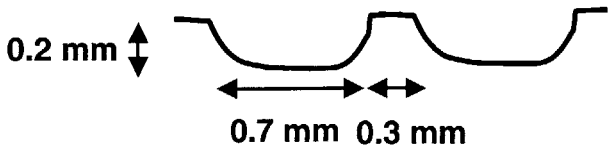

Figure 3-5: Dimensions of the grooved pattern

prior to bonding.

Patterning

The Precision Art Company in Springfield, MA provided the etching services. A photochemical etching procedure as described in Section 2.6 was used to etch grooves into the metal surfaces. The dimensions of the grooves were chosen to be on the order of the thickness of the adhesive. Figure 3-5 shows a diagram of the grooved pattern. Pictures of the actual metal (after bonding) can be seen in Chapter 4.

After the grooved metal was received, it was then sent to the Poly-Metal Finishing Co. to be primed with BR-127^{TM}Primer. This was done so that accurate comparisons could be made between the patterned metal and the baseline primed metal. Again, handling of the grooved and primed metal was kept to a minimum prior to bonding to avoid contamination. Note that for the DCB specimens, only the pre-cracked side of the specimen was grooved. Regular primed metal was used for the other side to save the extra photoetching cost.

3.3.2 Composite Surfaces

Different techniques were also used to prepare the composite surfaces. Although initially, the composite surface was assumed to be less important and less likely to fail, preliminary testing showed that the composite surface was often the limiting factor. The following sections will describe the different preparation methods employed.

As-Cured

After the composite laminates were cured, the surrounding cure materials (bleeder paper, GNPT, peel-ply, etc.) were immediately removed from the laminate. The bare laminates were then post-cured and cut to size as described in Section 3.2.4. Prior to bonding, the composite surfaces were brushed with a dry piece of cheesecloth. No chemicals or abrasives were used to further clean the surfaces. The curing materials leave a patterned imprint on the composite surfaces that was thought to be adequate for bonding.

Peel-Ply

This method is similar to the As-Cured case, except that in this method, the peel-ply layer was left on the composite surfaces after curing until just prior to bonding. This kept the surfaces very clean and free from dust. Nothing else was done to the surfaces prior to bonding.

Sanding

The composite surfaces were sanded with 80-grit sandpaper. This caused a significant amount of powder, greenish in color, to be removed from the surface. The surfaces were sanded until this greenish powder was removed and an evenly scratched, black surface was obtained. The surfaces were wiped with damp cheesecloth to remove most of the excess powder, and then they were wiped with dry cheesecloth until no more powder came off onto the cloth. Solvents were not used to clean the surfaces to avoid degrading or dissolving the composite. Care was taken to avoid contaminating the surfaces prior to bonding.

Co-Curing

Co-cured specimens have no composite surface preparation. The laminates are prepared as usual (see Section 3.2.4), and then the film adhesive is bonded directly to the pre-preg, which is sticky to the touch. It was assumed that during curing, the epoxy

in the pre-preg material and the film adhesive would mix, producing a strong bond. It should also be noted that most co-cured specimens were post-cured in a 350°F oven for 8 hours, although one set of specimens was not post-cured for comparison purposes.

3.4 Testing Procedures

The DLS specimens were mechanically tested on a MTS hydraulically actuated testing machine equipped with a 100,000 lb load cell. Pieces of emery cloth 3 inches long and 1 inch wide were taped to the ends of the specimens to provide a gripping surface. The specimens were placed in the machine and aligned using a square. The MTS machine was connected to a computer and data acquisition system so that load and position data could be recorded continuously by the LabView^{TM}software. The specimens were loaded in position control, at a rate of 0.01 inches per minute until failure. The maximum load reached was recorded automatically by the machine. The bond strength was calculated by dividing the maximum load reached by two times the average bond surface area (since there is a bond on either side), $\sigma_{bond} = \frac{P_{failure}}{2A_{average}}$.

The DCB specimens were tested on a MTS machine equipped with a 1,000 lb load cell. Aluminum strips were screwed onto the hinges to provide material for the testing machine to grip. The specimens were placed in the machine and aligned using a level. A picture of the test set-up is shown in Figure 3-6. The specimens were loaded in position control at a rate of 0.1 inches per minute. Load and position data were automatically recorded. The specimens were visually monitored constantly. Every time the crack grew and passed one of the measured markings on the side of the specimen, a notation was entered into the computer data stream. These data points were later used to calculate the strain energy release rate in the specimens. When the crack had progressed beyond the 30 mm mark, the specimens were unloaded and removed from the machine.

The critical strain energy release rate (fracture toughness) was calculated using a formula derived from the strain energy present within a cantilevered beam, which is

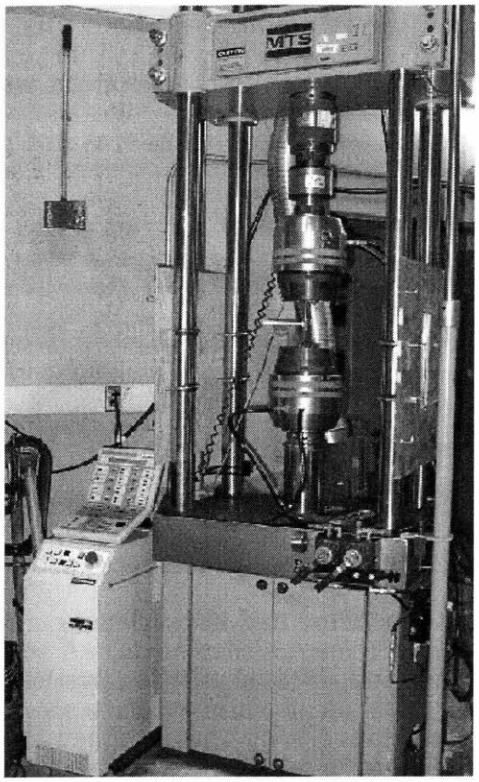

Figure 3-6: The testing machine set-up

defined as [29]

$$U = \int_L \frac{M_b^2}{2EI_{zz}} \mathrm{d}x \tag{3.1}$$

where L is the length of the beam, M_b is the bending moment, E is the modulus and I_{zz} is the moment of inertia of the beam. For the metal/composite joints, two "beams" were considered: a plain metal beam and a metal/composite hybrid beam. Solutions for a plain metal beam exist and are straightforward; the strain energy release rate is just the derivative of the strain energy with respect to the area of new crack surface, and can be expressed as

$$G = \frac{1}{b}\frac{dU}{da} = \frac{P^2a^2}{2bEI} \tag{3.2}$$

where P is the applied load, a is the crack length, and b is the width of the beam. The solution for the strain energy present in a hybrid beam was calculated using modulus weighted areas and moments of inertia. Superimposing these two solutions,

a formula for the strain energy in the double cantilever beam can be found. Taking the derivative of this expression, which is the same as Equation 3.2 but with new values for E and I, the strain energy release rate for the total DCB specimen is defined as

$$G = \frac{P^2 a^2}{bE^*}\left(\frac{1}{2I^*} + \frac{1}{2I}\right) \tag{3.3}$$

where E^* is the reference modulus (taken as the modulus of aluminum in this study) and I^* is the modulus weighted moment of inertia which was calculated to be

$$I^* = \frac{bh_1^3}{12} + \left[\frac{(h_1+h_2)\,h_2E_2}{2\,(h_1E_1+h_2E_2)}\right]^2 bh_1 + \frac{bh_2^3}{12}\frac{E_2}{E_1} + \left[\frac{(h_1+h_2)\,h_1E_1}{2\,(h_1E_1+h_2E_2)}\right]^2 bh_2\frac{E_2}{E_1} \tag{3.4}$$

where the subscripts "1" refer to the metal adherend and the subscripts "2" refer to the composite adherend. To find the *critical* strain energy release rate, the load and crack length right before failure were used.

The general equation for G for composite materials, as described in ASTM Standard D5528 [12], was not used because of its strong dependence on the crack tip opening displacement. Displacements in this study were measured solely from the cross-head displacement of the testing machine. Yielding in the hinges or slipping in the grips could have caused inaccuracies in this displacement measurement. Therefore, the approach outlined above using Equations 3.2 and 3.3, which does not use displacement measurements, was used exclusively in all calculations.

3.5 Test Matrix

All of these metal and composite surface preparation methods were combined to produce a test matrix. Table 3.4 shows which combinations were tested, and which adhesives were used. For the DLS tests, eight to ten specimens of each configuration were tested. Only four to six DCB specimens of each type were tested due to problems with the hinges.

Sanded metal co-cured joints were not made due to manufacturing difficulties. Unless primer was applied to the metal surfaces, the joints would not adhere during

Metal Surface	Composite Surface			
	As-Cured	Peel-Ply	Sanded	Co-Cured
Sanded	FM-123™	FM-123™	FM-123™ **FM-300™**	
Primed			FM-123™ **D**(FM-123™)	FM-300™ **Q**(FM-300™)
Anodized			FM-123™	
Grooved				FM-300™

Table 3.4: Test Matrix

the cure process. When the sanded specimens were removed from the autoclave, they were already fractured.

Three special tests are also indicated in this chart (notated in bold). First, a secondary cure was performed with sanded composite and primed metal, but using FM-300™film adhesive. This adhesive cures at 350°F and was used for all the co-cured specimens. The objective of this test was to see the effect of using two different adhesives, and of curing at different temperatures.

The second special test (indicated by the **Q**) was performed to examine the effect of the CTE mismatch. In this test, a quasi-isotropic laminate, which has a CTE that is closer to that of aluminum, was used to co-cure with primed aluminum. This will be discussed further in Section 5.5.

The third special test (indicated by the **D**) was performed to explore the reliability of the joints. In industry the technicians who construct the joints may not always take care to prepare the parts perfectly. Therefore, the effect of introducing faulty surface preparations on the adherends was studied. This was accomplished using three methods:

1. Sanding and wiping with acetone parts of the primed metal to remove the primer
2. Putting oil on parts of the metal surface
3. Leaving parts of the composite unsanded

Figure 3-7 shows the configurations of the defects on both the DCB and DLS specimens.

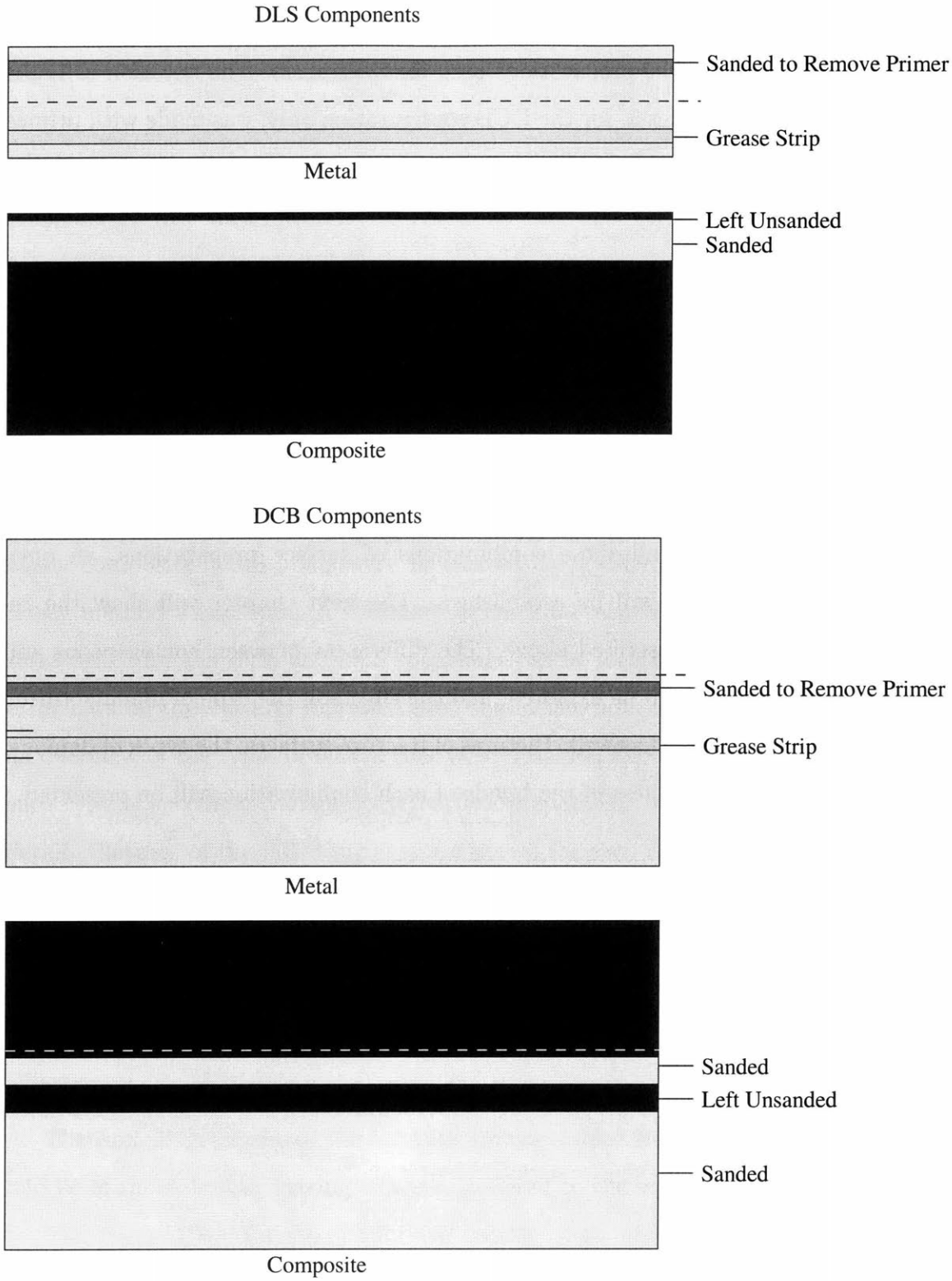

Figure 3-7: Diagram of simulated defect types and locations

Homogeneous tests were also performed. For these tests, metal/metal bonds and composite/composite bonds were manufactured with various surface preparations. Table 3.5 shows the surface preparations used for these tests. The notation **T DCB** indicates that one set of tests, for the DCB configuration only, was made with primed metal that was twice as thick (.125") as that used for all the other tests. The purpose of this was to avoid plastic deformation in the adherends. This will be discussed further in Section 5.2.

	Sanded	Primed
Composite/Composite	FM-123^{TM}	
Metal/Metal	FM-123^{TM}	FM-123^{TM} **T DCB**(FM-123^{TM})

Table 3.5: Homogeneous test matrix

By running tests on all these combinations of surface preparations, an optimum bonding procedure will be established. The next chapter will show the results from all the tests described above. The differences between homogeneous and metal/composite joints will be explored, and the effects of the type of manufacturing procedure will be discussed as well. Pictures of fracture surfaces, the types of damage, and the strength or toughness of the bonds of each configuration will be presented.

Chapter 4

Results

4.1 Overview of Results

Many composite-metal joints were fabricated using different methods before a preferred method was chosen. A summary of the final results of all the surface preparations tested for the DCB and DLS specimens can be seen in Figures 4-1 and 4-2. The error bars on these charts represent 95% confidence intervals. The next section gives an overview of the types of failure that were observed experimentally. Following this, each type of specimen configuration/surface preparation method will be described in detail. Pictures of the failed surfaces are shown for each case.

4.2 Failure Modes

Three different failure modes were observed during the experimental tests. Figure 4-3 diagrams these schematically.

The first diagram shows the cohesive failure mode. Here, the crack grows in the middle of the adhesive, leaving adhesive adhered to the surfaces of both adherends.

The second diagram shows adhesive failure. Here, the adhesive does not adhere to one of the adherends. The crack propagates along an adherend/adhesive interface. This is due to poor surface preparation on the adherend that does not adhere to the adhesive.

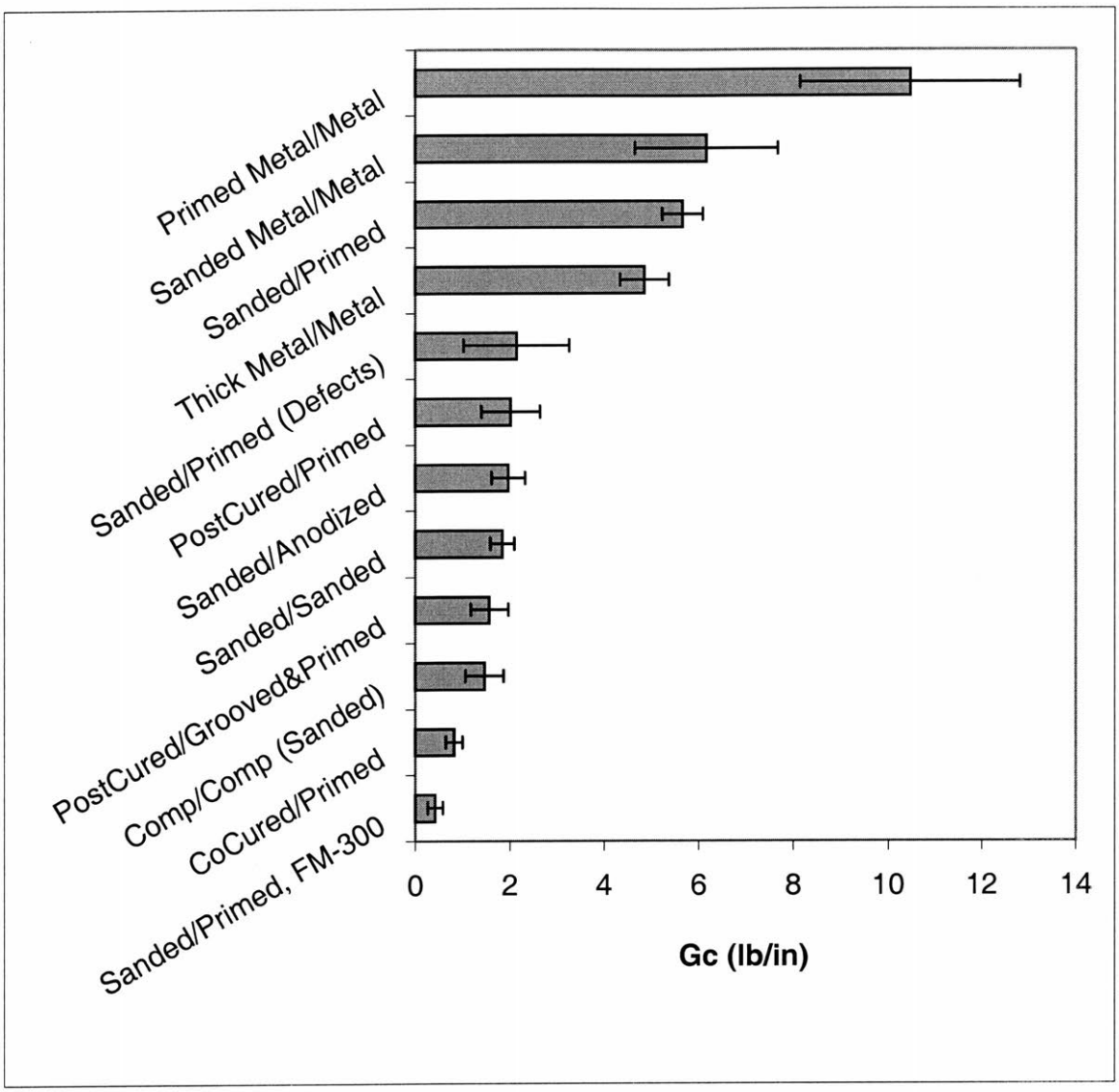

Figure 4-1: Summary of DCB results

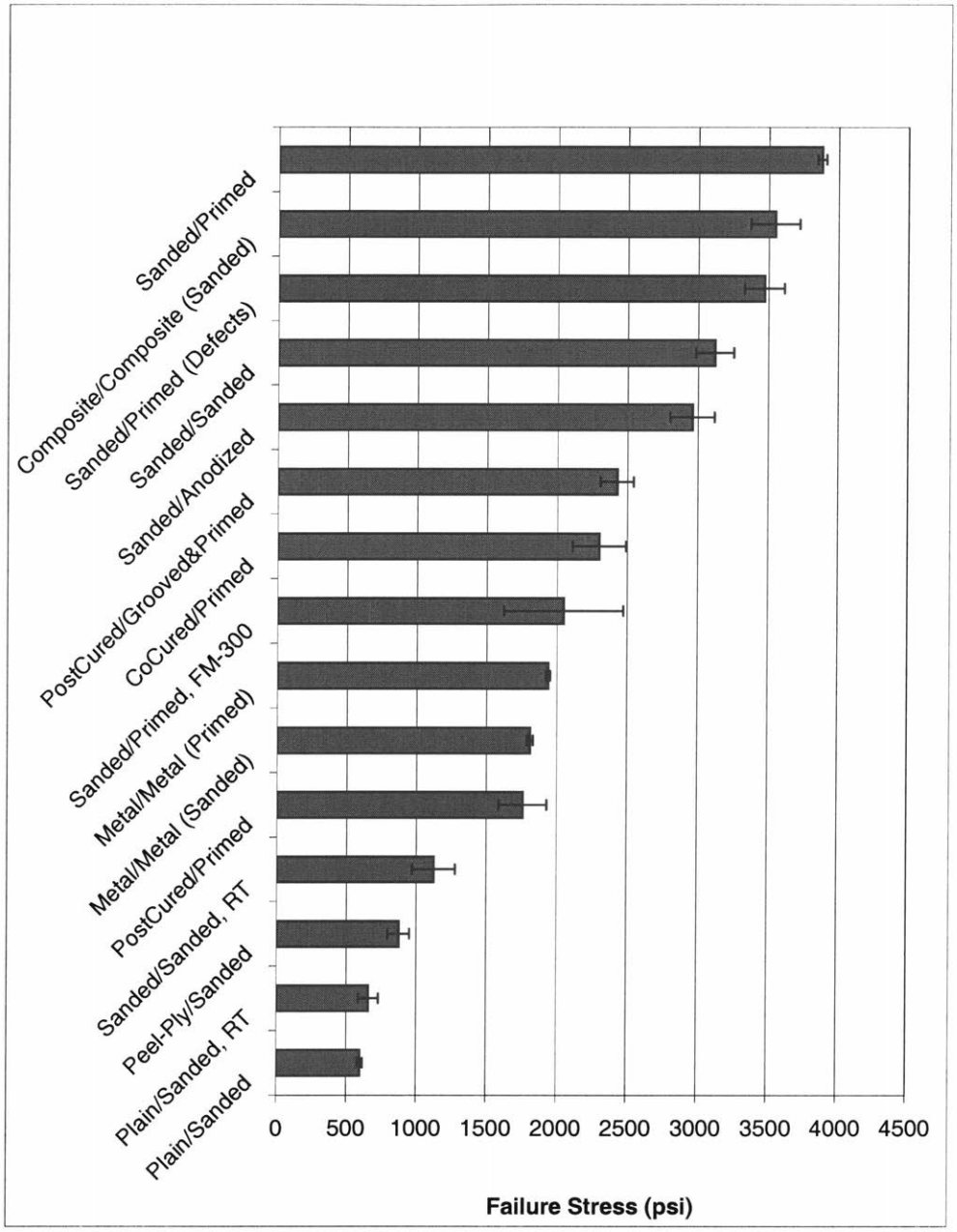

Figure 4-2: Summary of DLS results

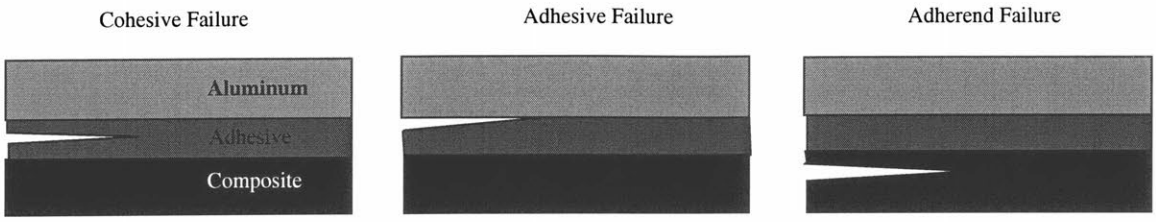

Figure 4-3: Diagram of the three failure modes

The last diagram shows adherend failure. Here, the specimen fails within one of the adherends itself. This usually took the form of delaminations within the composite adherends.

The following sections will describe the failure characteristics of each of the specimen types.

4.3 Composite Surface Preparation Effects

It was discovered early on that the composite surface preparation was crucial to the overall bond strength. It was observed (see Figure 4-2) that sanding the composite more than quadrupled the DLS bond strength over the as-cured and peel-ply configurations. The peel-ply surface left the composite cleaner than the as-cured surface, but did not increase the strength by a significant amount.

A paper by L. J. Hart-Smith [30] explains why the peel-ply surface performed so poorly. Hart-Smith studied several peel-plies and found that in order for them to be removed from the laminate after curing, they needed to be coated with a release agent. This release agent is transferred to the laminate during curing, leaving an unbondable film on the composite surface. Using non-release coated peel-plies makes it impossible to remove the peel-ply after curing. Therefore, Hart-Smith concludes that ALL composite surfaces that have been cured with peel-ply need to be mechanically abraded by sanding or grit blasting before bonding or painting.

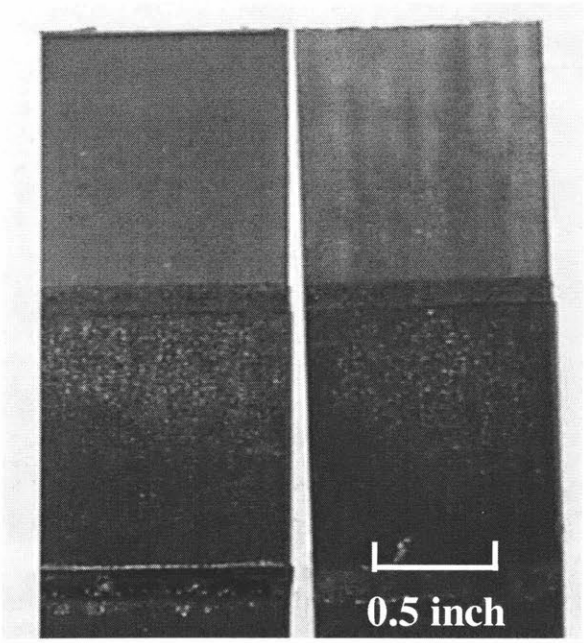

Figure 4-4: A fractured as-cured DLS specimen

Figures 4-4, 4-5, and 4-6 show pictures of the fracture surfaces of the as-cured, peel-ply, and sanded specimens (all with sanded aluminum), respectively. These pictures show two different failure modes (as described in Section 4.2). The as-cured and peel-ply specimens failed at the adhesive/composite interface, leaving no adhesive adhered to the composite surface. In contrast, cohesive failure (within the adhesive) was observed on the sanded composite specimens. The cohesive failure proves that adhesive was adhering to both the metal and composite surfaces, and therefore the surfaces were prepared adequately.

Figure 4-7 shows a load-displacement curve for a representative sanded/sanded specimen. The curve is predominately straight, with little to no evidence of any yielding taking place.

The DCB specimens showed similar results. Two of the un-sanded (as-cured) specimens unbonded a significant distance just from the thermal stresses alone. This suggests once again that un-sanded composite surfaces are inadequate.

In some cases, the hinges were pulled off the specimen before fracture began. When the hinges stayed on, the bonds all broke in the same fashion. First, the crack would initiate and grow a large distance all at once, causing the load to drop dramatically.

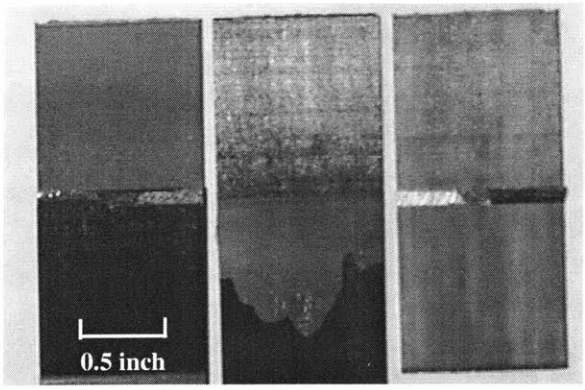

Figure 4-5: A fractured peel-ply DLS specimen

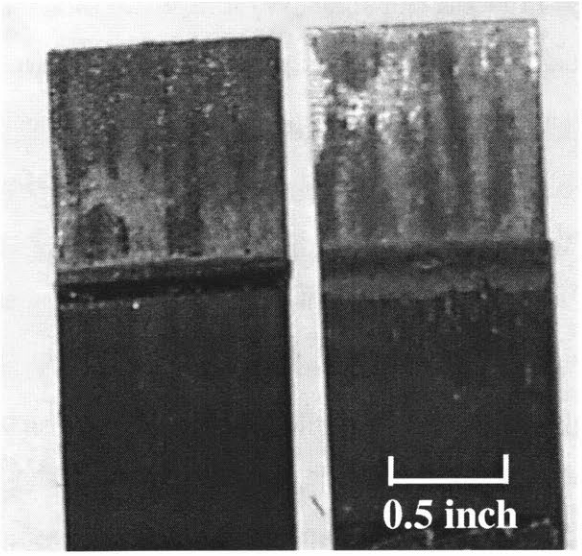

Figure 4-6: A fractured sanded DLS specimen

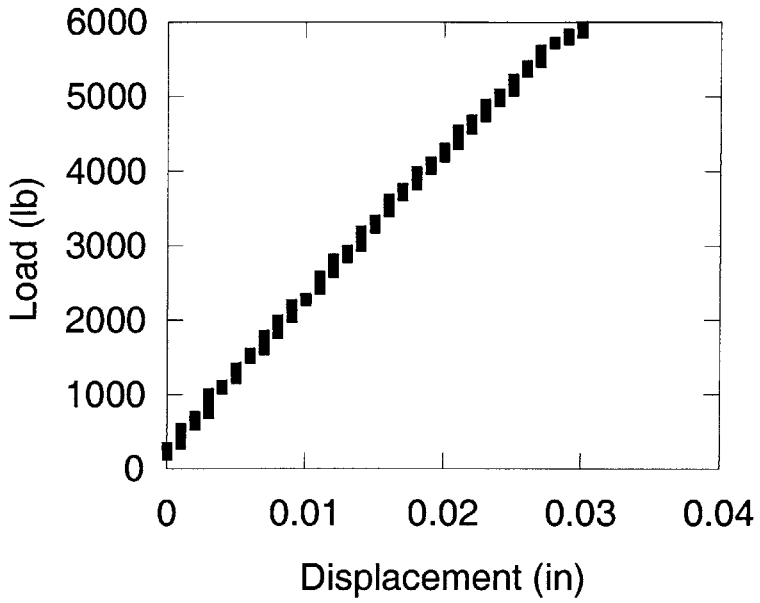

Figure 4-7: Load-displacement curve for a sanded/sanded DLS specimen

This was termed "catastrophic failure". As the load increased, the crack propagated more slowly along the remainder of the bond line.

The un-sanded specimens fractured at the composite/adhesive interface, so that all the adhesive remained glued to the metal adherends. A picture of this can be seen in Figure 4-8. Notice here that the composite surface is absolutely bare.

The specimens with sanded composite adherends broke, for the most part, a ply or two into the composite adherend. Often, the crack would initiate cohesively in the adhesive layer, but then the composite would begin to delaminate, and the crack would propagate into the composite.

4.4 Primed Specimens

The initial DCB test results for primed metal/sanded composite were similar to the sanded metal/sanded composite results from before. Here, the joints fractured catastrophically, producing a crack along almost the entire length of the specimen. Because there was no more room to propagate the crack, only initiation values of the strain

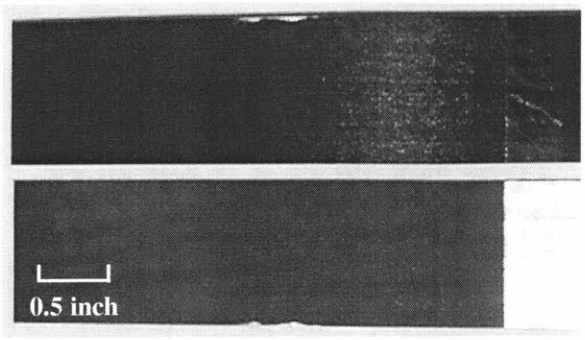

Figure 4-8: A fractured as-cured DCB specimen

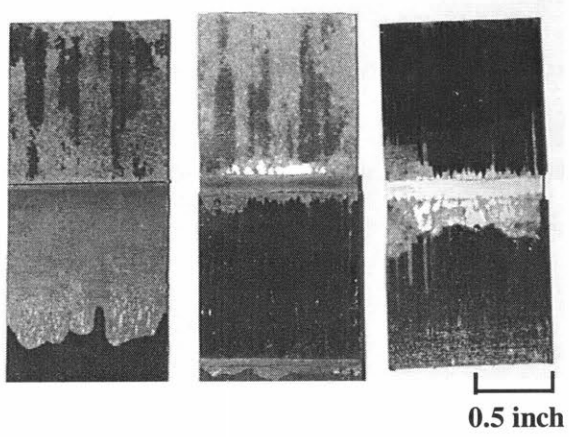

Figure 4-9: A fractured primed DLS specimen

energy release rate could be calculated. The primer produced bonds strong enough such that the metal adherends began to yield before the crack propagated.

The BR-127 primer had a dramatic effect on the strength of the DLS specimens. An average strength increase of more than 700 psi over the regular sanded specimens was observed. Generally, cohesive failure within the adhesive layer was observed, as seen in Figure 4-9. In some cases, pieces of the composite were adhered to the adhesive surface, as seen in the rightmost part of Figure 4-9. This once again shows that a good adhesive bond was created. Interestingly, it was noted that the specimens did not fail until after the metal doublers had been loaded beyond their yield strength.

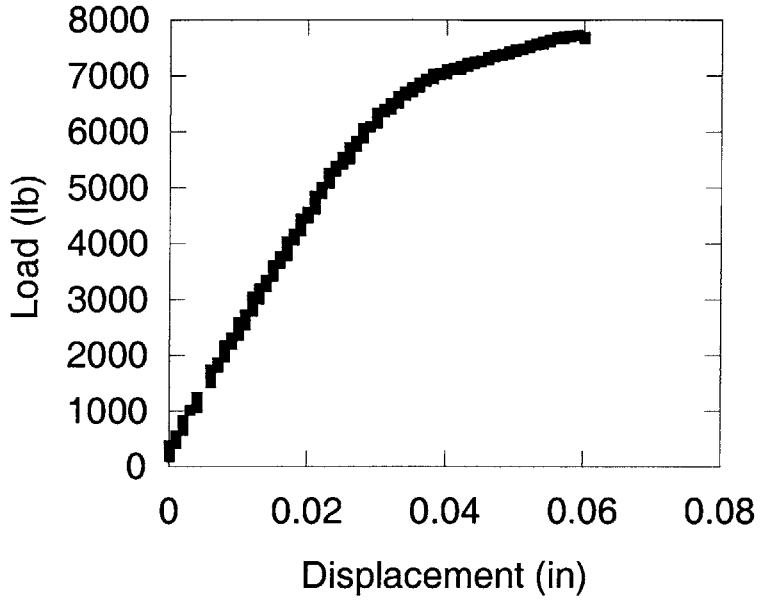

Figure 4-10: Load-displacement graph of primed metal DLS specimens

This can be seen by observing the load-displacement graph in Figure 4-10, which shows obvious non-linear characteristics. Furthermore, the metal doublers themselves deformed plastically, and this can be easily seen in the "necking" observed in all the failed specimens, as shown in Figure 4-11.

4.5 Anodized Specimens

Specimens were made by the secondary curing process using sanded composite laminates, anodized metal, and FM-123^{TM}film adhesive. The DLS specimens showed disappointing results. The failure strengths of these bonds were considerably less than those of the primed metal, and were similar to those of the sanded metal. About half the bonds broke cohesively, within the adhesive layer itself. In some cases, a few fibers were adhered to the metal surface, but in general the bonds did not fail within the composite adherend. Some adhesive failure at the metal surface was also observed. These combined failure modes can be seen in Figure 4-12, which shows a magnified view of one of the composite adherend bond surfaces. Notice how the left part shows

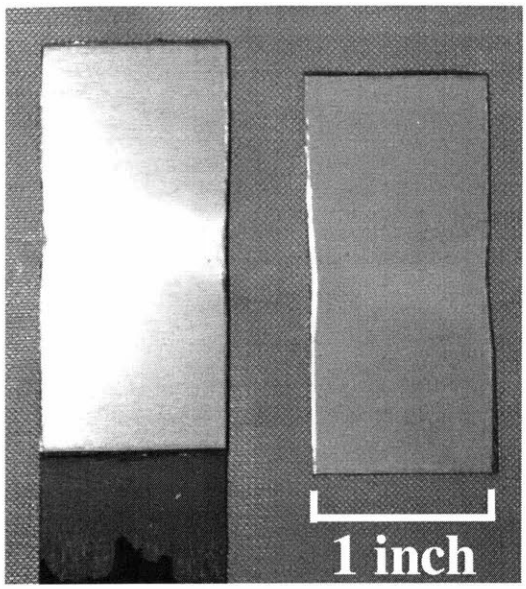

Figure 4-11: Evidence of yielding in primed metal DLS specimens

all the adhesive adhering to the composite, while on the right, some composite fibers have been broken away. This was an unusual result; in no other specimen type was there such a marked mixture of failure modes as shown here. This type of failure suggests that parts of the anodized metal surface did not adequately adhere to the film adhesive, thus leaving a clean fracture surface as shown on the left side of Figure 4-12. However, part of the metal *did* adhere well, as shown by the composite fiber damage on the right side of the figure. Here, fibers have been pulled away, and remained adhered to the metal surface. Hardcoat anodizing, therefore, does not seem to be a consistent or reliable surface preparation method for metal/composite joints.

The DCB specimens performed about as well as many of the co-cured specimens. There was not as much yielding as the primed specimens. The bonds did tend to break catastrophically, and mostly delaminated within the composite after initiating in the adhesive.

4.6 Manufacturing Defects

The DLS specimens with manufacturing defects had strengths only slightly less than the regular primed/sanded specimens. The defects did change the failure mode

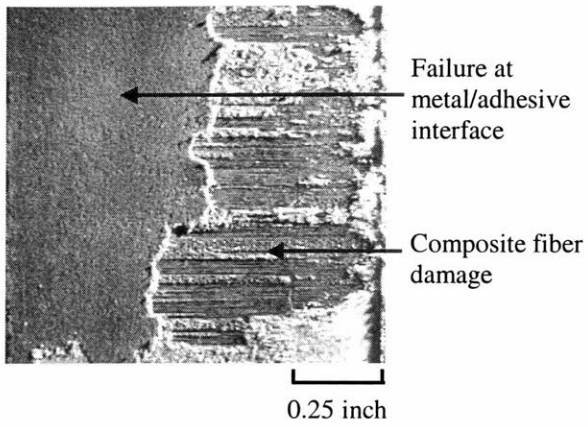

Figure 4-12: Magnified view of the fractured anodized surface

slightly, however. In some cases, the adhesive did not adhere well to the metal surface in the spots where the primer was removed. Also, the adhesive did not stick to the parts of the composite adherends that were not sanded. This was consistent with previous results for the un-sanded composite specimens. For the most part, however, the bonds failed cohesively, similar to the regular primed/sanded specimens. Figures 4-13 and 4-14 show the fracture surfaces.

There is evidence of a small amount of yielding in the metal doublers as seen in Figure 4-13. Notice in Figure 4-14 the bare part of the composite at the edge, where it was not sanded. Also notice the smooth part on the bottom center of the adherend where the adhesive completely adhered to the composite. This is where the primer had been removed from the metal surface.

The defect DCB specimens did not show any visual response to the presence of defects. The specimens all failed completely by composite delamination. In all cases, a layer of composite fibers was left adhered to the metal surface. The bonds also broke catastrophically, often breaking in spurts, several millimeters at a time. The unsanded regions did not seem to have any effect on the failure mode, since the bonds did not fail at the composite/adhesive interface as expected. This is probably due to the fact that the crack initiated within the composite since the beginning of the composite bond area was sanded. It would then be difficult for the crack to jump

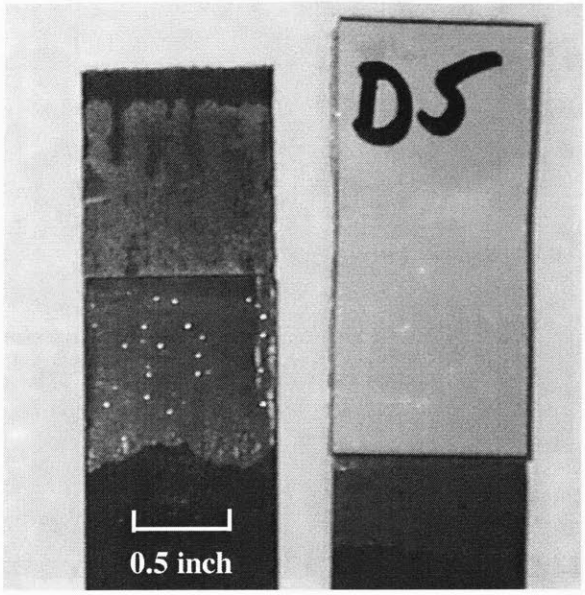

Figure 4-13: A fractured defect DLS specimen

from composite delamination to adhesive failure at the composite/adhesive interface.

The DCB specimens showed very scattered fracture toughnesses, but with an average value significantly less than the regular sanded/primed specimens. This suggests that the placement of bond defects did cause the specimen to delaminate faster than expected.

4.7 Homogeneous Tests

Composite/Composite and Metal/Metal DLS and DCB specimens were constructed to investigate how joints made with the same materials behave. The DLS composite joints performed extraordinarily well, with failure strengths surpassing all those tested except the primed/sanded specimens. Sanded and primed metal/metal joints performed about the same in the DLS tests, and had the weakest joint strengths of all the secondarily-cured specimens. All the homogeneous joints of both materials failed cohesively, that is, within the adhesive layer. Figures 4-15 and 4-16 show fractured composite and primed metal homogeneous specimens, respectively.

The metal/metal DLS joints showed evidence of yielding as well. Figure 4-17 shows a load-displacement plot exemplifying this.

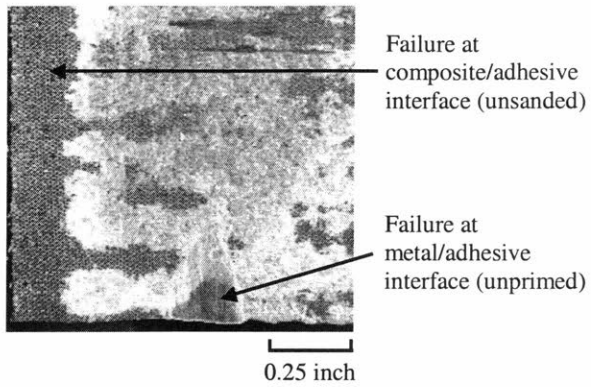

Figure 4-14: Magnified view of a fractured defect DLS specimen

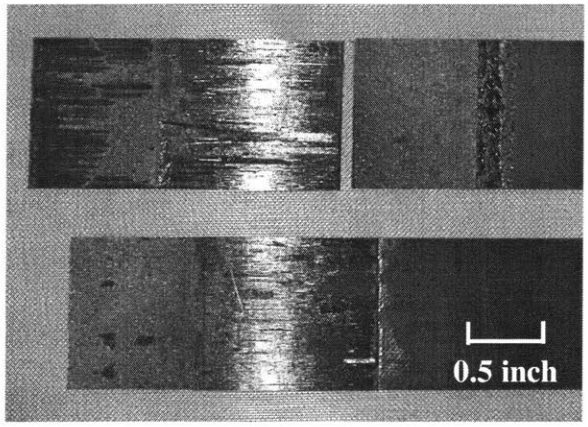

Figure 4-15: A fractured composite DLS specimen

The DCB results were quite different from the metal/composite joints tested previously. In both the all-metal and all-composite specimens, the crack initiated and propagated slowly; there were no large jumps. This was called "progressive" failure, and will be discussed further in Section 5.3. The metal adherends yielded a significant amount, producing a crack opening displacement of almost 3 inches. Figure 4-18 shows a side view of a fractured specimen, with yielded adherends. Because of this large amount of yielding, the calculated fracture toughnesses were abnormally high (see Figure 4-1), and are most likely not valid measurements. This will be discussed further in Section 5.2.

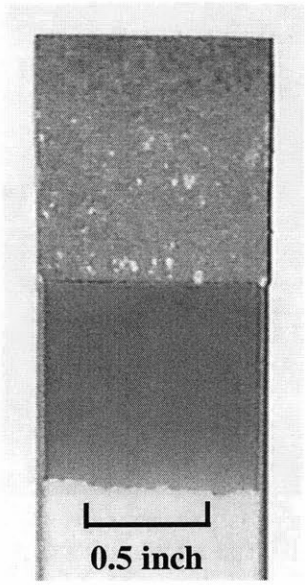

Figure 4-16: A fractured primed metal DLS specimen

The thick (0.125") primed metal DCB specimens reached a maximum load more than twice that of any of the other configurations tested. This high load caused the hinges that were bonded to the specimens to break off before the specimens fractured. Therefore, holes were drilled and tapped into the metal adherends, and the hinges were screwed on. Small washers were used as spacers such that the small screws did not penetrate into the opposite adherend. This method worked extremely well; the hinges were free to rotate and remained on the specimens for the duration of the tests. The specimens all broke cohesively and progressively, and there was no evidence of yielding. The calculated fracture toughnesses were much lower than those of the thin primed metal/metal, as expected.

4.8 Co-Cured Specimens

In order to investigate the interaction of the film adhesive mixing and curing with the epoxy embedded in the graphite pre-preg, co-cured joints were manufactured. A higher-temperature film adhesive, FM-300^{TM}, was used because the composite must

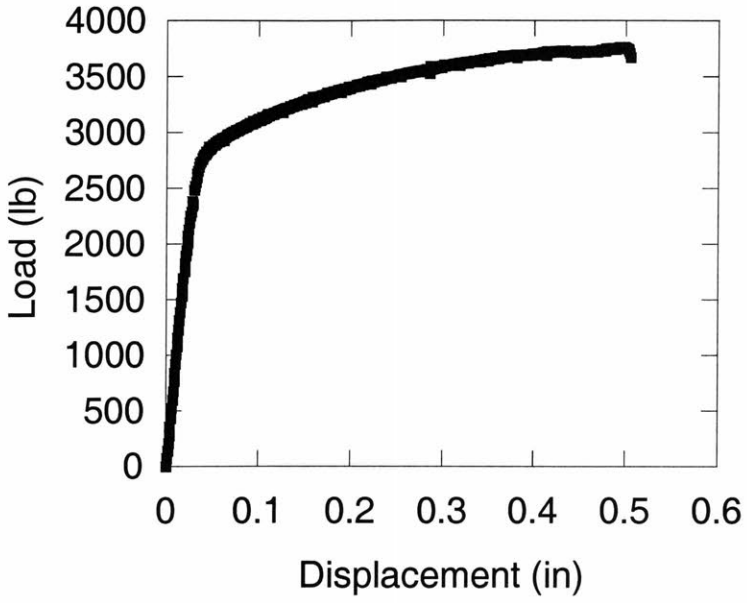

Figure 4-17: Load-displacement plot for a primed metal/metal DLS specimen

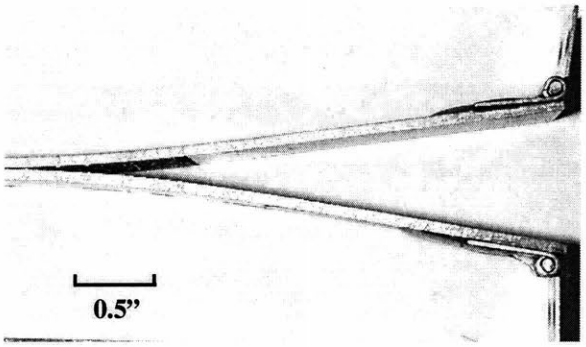

Figure 4-18: A yielded primed metal DCB specimen

be cured at a temperature of 350°F. Unfortunately, preliminary tests showed that the plain, sanded metal adherends often did not bond to the composite using this method. One theory as to why this happened is that the high temperature cure cycle may have caused too much stress to be stored in the joint, and the bond broke during cool-down.

However, when primed aluminum was used, satisfactorily bonded co-cured joints were made. Specimens of both DLS and DCB types were manufactured. The dimensions of these specimens were slightly smaller than the previously manufactured specimens due to the extra trimming that was required after co-curing. These changes should not have affected any of the test data.

The co-cured DLS specimens showed disappointing strength results. The average failure load was slightly less than 2000 psi, which is significantly lower than the secondarily cured specimens with and without primed metal adherends. All of the bonds broke about one ply into the composite adherends. That is, pieces of composite were adhered to the metal/adhesive layer in all cases. Figure 4-19 shows this failure within the composite adherend. This shows that the composite itself is the limiting factor in the strength of the joint. One factor that may have influenced this result is that these co-cured joints were not post-cured before testing. This may have caused the composite plies to delaminate prematurely.

The co-cured DCB specimens showed similar results. This time, the surfaces where the hinges were applied were first scrubbed with acetone and sanded with 80-grit sandpaper before bonding the hinges with 5-minute epoxy. The failure loads were quite low, and the corresponding strain energy release rates were also low. After initiation, the cracks almost immediately turned into the composite laminate, delaminating the specimen several plies away from the interface. Figure 4-20 shows a higher magnification view of the side of a DCB specimen. The delaminations within the composite can be clearly seen here.

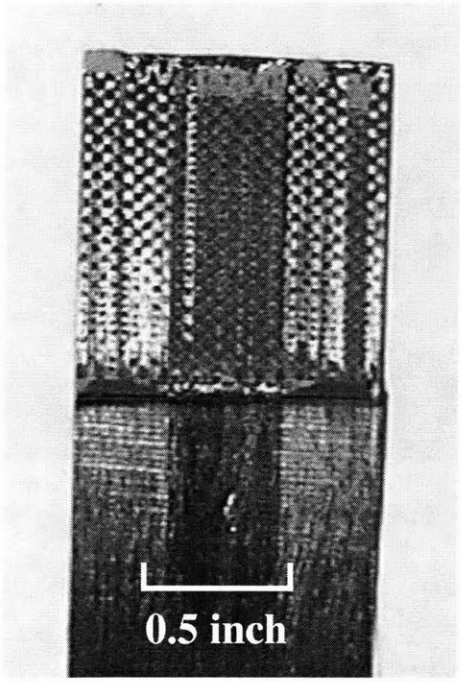

Figure 4-19: The composite adherend of a co-cured specimen

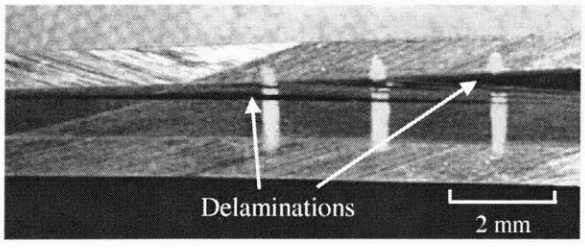

Figure 4-20: Side view of a co-cured DCB specimen

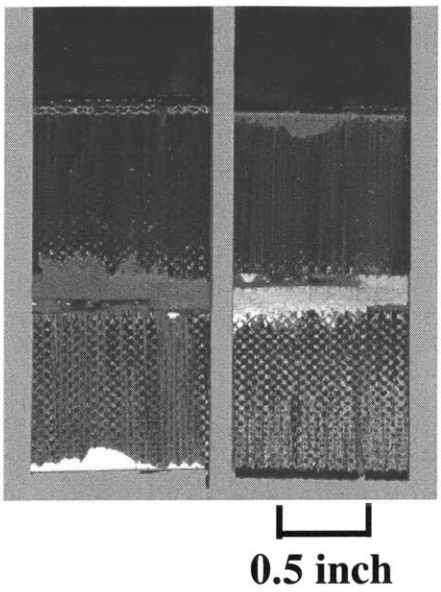

Figure 4-21: A fractured post-cured DLS specimen

4.9 Post-Cured Specimens

These specimens are the same as the Co-Cured ones, except that this time they were post-cured in an oven for 8 hours at 350°F. Some extra DCB specimens from the previous batch of co-cured specimens were post-cured as well. These specimens were then tested in the normal manner. The DLS tests showed slightly worse results after the post-curing process (see Figures 4-2). This could have been caused by more thermal residual stresses being locked into the joints. A picture of the fracture surfaces can be seen in Figure 4-21. Notice the large amount of damage done to the composite adherend. Many of the fibers were broken and remained adhered to the metal surface. The DCB specimens showed improvement, however, doubling the critical strain energy release rate of the co-cured specimens.

4.10 Grooved Specimens

A close-up view of the grooves before testing can be seen in Figure 4-22.

The grooved DLS specimens produced quite interesting results. A majority of the

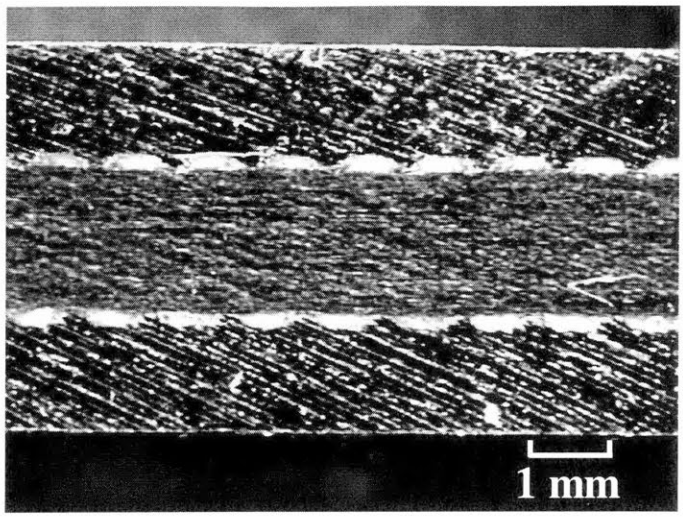

Figure 4-22: A grooved specimen

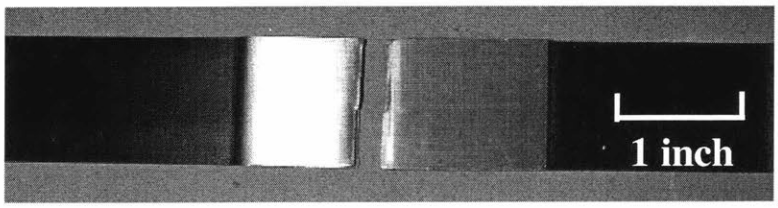

Figure 4-23: A failed grooved DLS specimen

specimens actually broke in half, shearing the metal doublers all the way through, as seen in Figures 4-23 and 4-24. In these cases, the metal yielded and failed before the adhesive joints debonded. This would seem to suggest that the bonds are performing extraordinarily well. However, the metal failed at a lower load than expected. Where previous results with un-grooved metal showed only yielding, the grooved metal showed fracture at the same loads. This suggests that the grooves in the metal may have caused stress concentrations which caused the metal to fail at a lower load.

The grooved DCB specimens showed almost no change in toughness as compared to the unpatterned, co-cured specimens (see Figure 4-1). A picture of a failed DCB

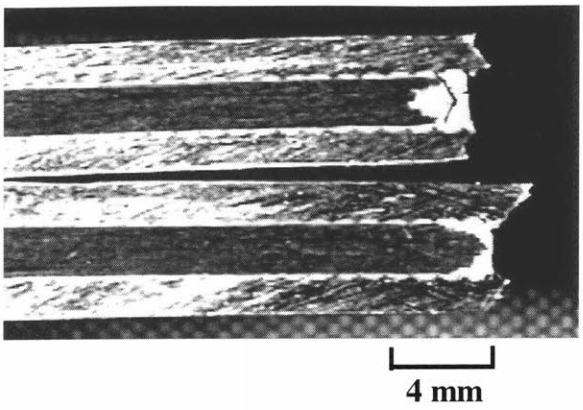

Figure 4-24: Magnified view of a failed grooved DLS specimen

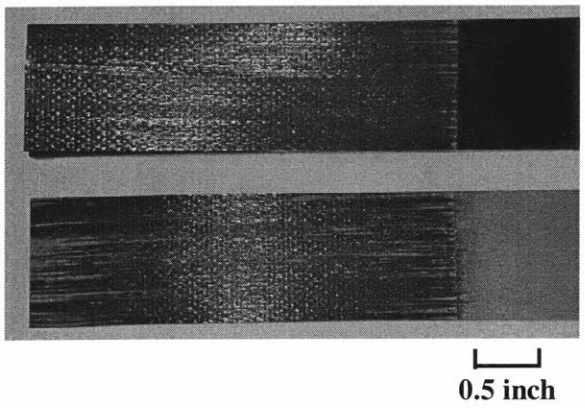

Figure 4-25: A failed grooved DCB specimen

specimen can be seen in Figure 4-25. Notice that a significant amount of composite fibers delaminated from the composite adherend and adhered to the metal/adhesive side.

4.11 High Temperature Secondary Cure

Two different adhesives, at two different curing temperatures, were used in this study. Therefore, tests were devised to compare the two. DLS and DCB specimens were made using primed metal, sanded (pre-cured) composite, and FM-300^{TM}adhesive.

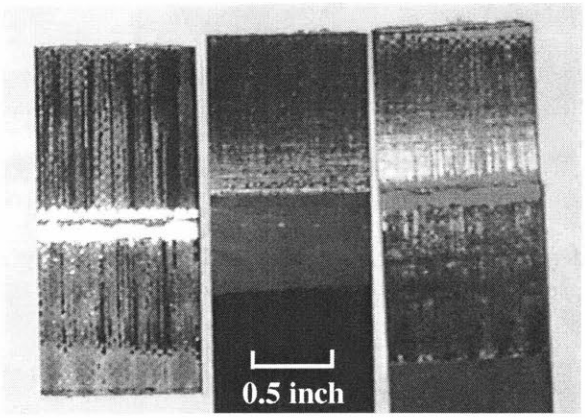

Figure 4-26: A failed high-temperature secondary-cure specimen

These specimens were secondarily cured using the standard graphite/epoxy cure cycle with a maximum temperature of 350°F. All the other secondary cures previously performed were made with FM-123^{TM}and cured at a lower temperature. Therefore, it was hoped that these tests would give insight into the effects of increasing the cure temperature as well as comparing the differences between the adhesives themselves.

The DLS data were quite scattered, but the failure strength results were on average very similar to the co-cured specimens tested previously, and considerably below the specimens that were cured with FM-123^{TM}(see Figure 4-2). This seems to suggest that either the adhesive FM-300^{TM}itself is significantly weaker than its lower curing temperature counterpart, or that the thermal residual stresses due to the higher temperature curing process degrade the joint strength. The published values of shear strength for the two adhesives only differ by 70 psi, so the effect is most likely due to the thermal residual stresses in the joint. The fracture surfaces displayed some composite fibers adhering to the metal and adhesive as usual, but not to the extent of the co-cured specimens (see Figure 4-26). There was no evidence of metal yielding.

The DCB data was also very similar to the co-cured results. The bonds did tend to break catastrophically, and delamination within the composite adherend was common.

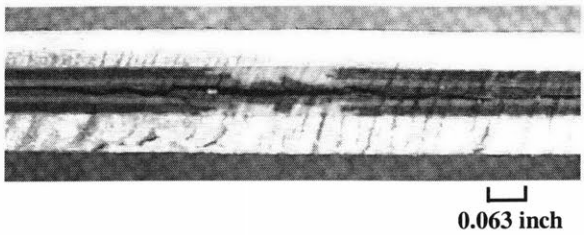

Figure 4-27: Delamination in a quasi-isotropic specimen

4.12 Quasi-Isotropic Laminates

All of the composite panels used so far in this study have been unidirectional laminates. While this provides a good method of studying the worst-case scenario in terms of CTE mismatch between the composite and the aluminum, unidirectional laminates are impractical in industry. Therefore, the effects of changing the laminate lay-up directions were then investigated. A more suitable stacking sequence which provided a compromise between stiffness and CTE was developed. The lay-up chosen was quasi-isotropic, $[0_2/\pm 45_2/90_2]_s$. This lay-up gave the least amount of CTE mismatch of the candidate materials examined (see Section 5.5.1 for a comparison of different lay-ups). Zero degree plies were maintained on the outside surfaces to give the same bonding surfaces as previous specimens.

DLS and DCB specimens were co-cured using this new composite lay-up with primed aluminum. However, once the specimens were cut, it was observed that the specimens were delaminated within the composite adherends, before they were tested. Figure 4-27 shows a picture of this delamination. This effect will be discussed further in Section 5.5.1.

4.13 Summary

Experimental results in the form of shear strength and fracture toughness data have been presented for each specimen type. These results show that the quality of the joint is highly dependent on the surface preparation as well as on the manufacturing method. From this data, it can be seen that the best overall bonding method is to

secondarily cure the specimens, with primed metal and sanded composite adherends. The novel patterning approach did not seem to have a positive effect on the quality of the joint.

The surface preparation method also effects the failure mode of the specimen. Furthermore, it is evident that the temperature change during the curing process has an effect on the properties of the joint because of the CTE mismatch between the two materials. The next chapter will discuss in more detail the failure modes and the thermal and plasticity effects that were observed experimentally.

Chapter 5

Analysis and Discussion

5.1 Introduction

In this chapter, all the issues that arose during the testing process are analyzed. First, the effect of plasticity on the fracture toughness of some of the DCB specimens is discussed, and three different methods are employed to better understand this effect.

Secondly, a discussion of the different types of failure is presented. The differences between adherend, adhesive, and cohesive failure are discussed. Also, an explanation of progressive versus catastrophic failure in the DCB specimens is given. Each specimen type is then classified as having one or more of these failure modes.

An analysis of the effects due to thermal and stiffness imbalances, based on the work of Hart-Smith described in Chapter 2 and applied to the particular specimens in this study, is then presented. Further thermal analyses, comparing different composite lay-ups, and also analyses based on Shetty's [16, 31] work are then described.

The chapter concludes with a discussion of the effects of patterning the metal surfaces.

5.2 Plasticity Effects

Yielding was observed in the metal/metal homogeneous DCB experiments. This plasticity may be responsible for producing abnormally high values of fracture toughness. Some yielding was also observed in the sanded composite/primed metal DCB bonds. In order to account for this effect, three different methods were used to estimate the true fracture toughness.

5.2.1 Thicker Adherends

First, an experimental approach was taken. Thicker sheets of aluminum (0.125" thick) were purchased and primed to use in DCB tests. The thicker metal would be less likely to yield before the crack propagated, and thus plastic deformation could be avoided. This data could then be compared to primed metal/primed metal DCB joints of regular thickness to compare directly the effect of plastic deformation on the fracture toughness of the joint. Unfortunately, this method would not work with metal/composite joints. Increasing the metal thickness in these bi-material joints would increase the thermal residual stresses that would be locked into the joint. This could potentially cause the specimens to fracture during the cool-down stage of the cure process.

5.2.2 Thouless Method

The second method was to incorporate analyses performed by other researchers to account for the energy absorbed due to plasticity. As mentioned previously, Thouless et.al. wrote several papers [32, 33, 34] on the toughness of plastically deforming joints. The researchers performed experimental and numerical analyses using wedge-impact and peel tests. They were able to correlate the fracture toughness of the bond to the resulting radius of curvature of the fractured specimen when using these constant-moment tests. They also presented a formula for calculating the toughness of bonds using the applied moment at the point of failure; this can be applied to the DCB tests used in this study even though they are not constant-moment tests. The

fracture toughness is expressed as

$$G = \frac{4M_p n}{b(n+1)} \left[\frac{2(n+2)M_p}{Abh^{n+2}} \right]^{\frac{1}{n}} \tag{5.1}$$

where M_p is the bending moment at failure, b is the width of the specimen, n is the strain hardening exponent, A is the strength coefficient, and h is the thickness of the adherends.

In order to use this formula, the stress-strain law of the metal must be known. In particular, the strain hardening exponent and the strength coefficient corresponding to the power law relationship between stress and strain of the form

$$\sigma = A\epsilon^n \tag{5.2}$$

must be known. These quantities can be calculated by performing a simple tensile test using a strain gage. The procedures for calculating the strain hardening exponent and the strength coefficient are documented in ASTM standard number E646 [35]. When this test was performed, a strength coefficient of 95 ksi and a strain hardening exponent of 0.155 were measured. Figure 5-1 shows the stress/strain curve for the primed metal that was used to obtain these values.

5.2.3 FEA Method

The third method was to perform a Finite Element Analysis on a model of a metal/metal DCB specimen. A model was created and processed in ABAQUS^{TM}. By performing a plastic analysis using the stress/strain data mentioned above, the amount of plastic strain energy in the joint at the time of fracture can be calculated. This can then be subtracted from the total energy to find the strain energy release rate or fracture toughness of the joint, which can then be compared to experimental data.

The relevant material properties and model data are tabulated in Table 5.1. Figure 5-2 shows a schematic of how the DCB joint was modeled. Only the lower half of the joint was modeled due to symmetry.

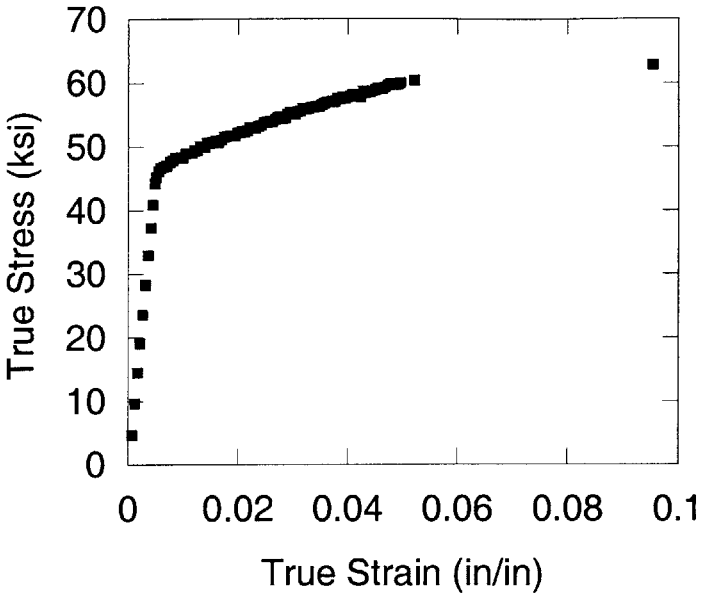

Figure 5-1: Stress/strain curve for primed metal

Material Properties	
FM-123 Modulus	342 ksi
FM-123 Poisson's Ratio	0.3
Adhesive Thickness	0.007 in
Aluminum Modulus	10,500 ksi
Aluminum Poisson's Ratio	0.33
Aluminum Yield Stress	46,893 psi
Aluminum Thickness	0.063 in
Model Properties	
Number of Nodes	25218
Number of Elements	8125
Element Type	8-noded shell elements
Initial Crack Length	2.42 in
Applied Load	19.2 lb
Yield Criterion	von Mises

Table 5.1: FE model properties

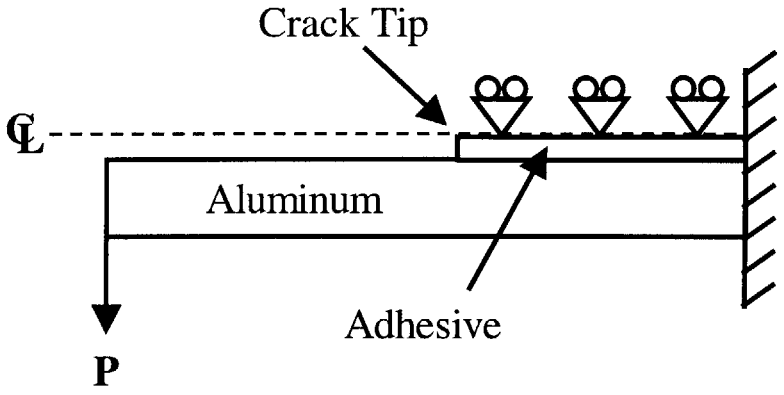

Figure 5-2: Schematic of FE DCB model

	Experimental	**Theoretical**	**Numerical**
Deflection (in)	0.47	0.43	0.46
G_c (lbin)	11.29	10.33	11.04

Table 5.2: Elastic analysis comparison

First, a purely elastic model was run to compare with simple beam theory to ensure the model was running properly. For this analysis, a homogeneous mesh was used, with 10 elements through the thickness of the beam. The material properties and dimensions were all as above with the exception that the aluminum was assumed to be elastic throughout. Table 5.2 compares the experimental, theoretical (from classical beam theory), and numerical (from ABAQUS^{TM}) results. These numbers seemed to match well, so a new model taking aluminum plasticity into account was analyzed.

Several models were made using different mesh refinements before a suitable mesh was found. Earlier meshes were either too coarse to obtain smooth stress contours or had discontinuities due to abrupt changes in mesh size. Figure 5-3 shows the final mesh that was used, "zoomed in" on the crack tip. A biased mesh was used such that the regions where the highest stress was expected had the smallest element sizes. That is, the top and bottom surfaces of the metal had finer meshes than the centerline, and the region near the crack tip was finer than the regions on the outer edges of the joint.

The maximum displacements just prior to failure are shown in Figure 5-4. The tip

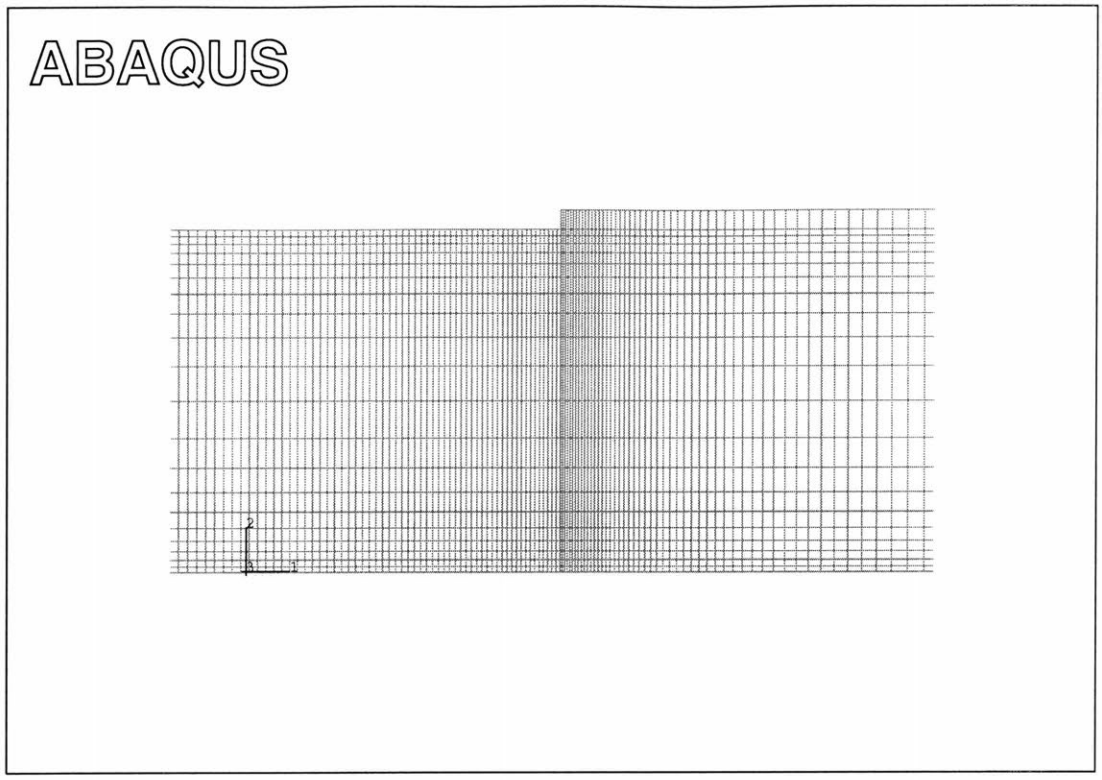

Figure 5-3: ABAQUS mesh used in plasticity studies

displacement calculated by ABAQUS^{TM}at failure is 0.6 inches, which is 28% higher than the experimental value of 0.47 inches.

ABAQUS uses the von Mises stress criterion to determine when the structure will yield. In this case, the uniaxial yield stress for aluminum that was used as input for the model was 46900 psi. Figure 5-5 shows Mises stress contours near the crack tip. The highest stresses occur nearest the crack tip, as expected. There are large regions where the Mises stresses are greater than the yield stress, indicating plastic deformation in the aluminum.

The code was run five times, each time "growing" the crack a small amount by releasing the boundary conditions on nodes representing the adhesive layer near the crack tip. After each run, the strain energy, plastic energy, and maximum deflection were recorded. The strain energy release rate was calculated from the formula

$$G = \frac{1}{B}\frac{dU}{da} \tag{5.3}$$

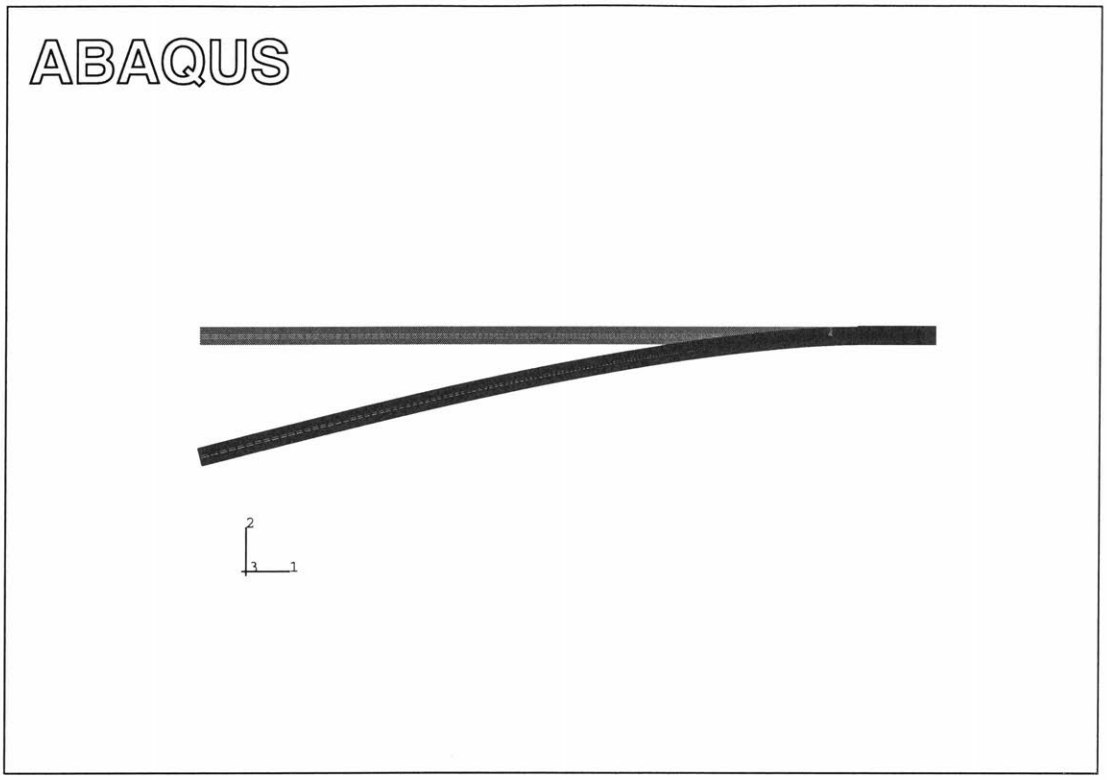

Figure 5-4: Displacement of lower metal adherend at failure

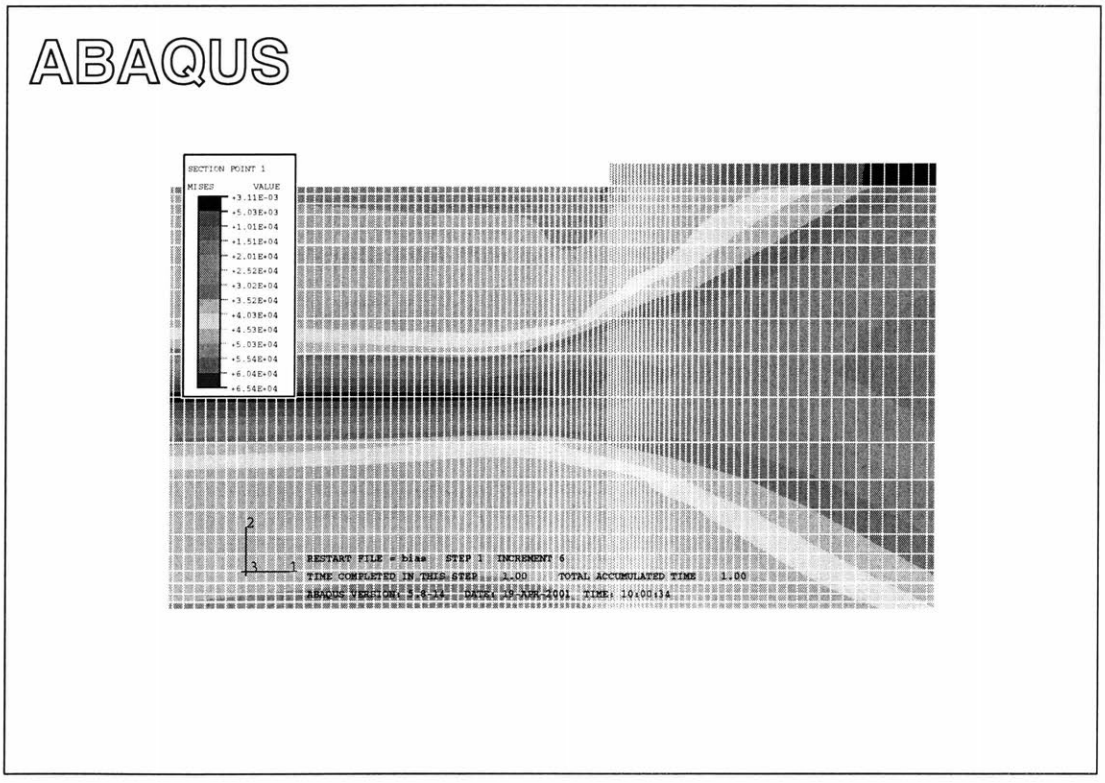

Figure 5-5: Mises stress contours near the crack tip

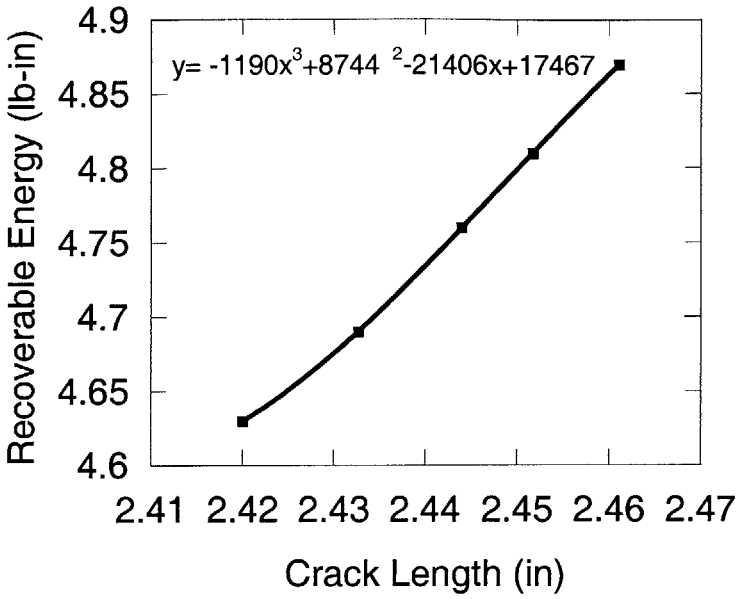

Figure 5-6: Plot of energy vs. crack length from plastic FE analysis (Note shortened scales)

where U is the recoverable energy (strain energy minus the energy due to plastic dissipation), a is the crack length, and B is the width of the joint. Table 5.3 summarizes the energy and displacement data that was obtained for each run of the simulation. By plotting U versus a, fitting a curve through the data points, and taking the derivative, the strain energy release rate can be calculated. By substituting for the initial crack length, the critical strain energy release rate for failure can be found. Figure 5-6 shows the U vs. a plot that was used in this analysis. The equation that was fit to the data is shown on the plot as well.

5.2.4 Results

The results using each of these methods are compared in Table 5.4.

These results show that the original thin metal experimental results produced G_c values that were too high due to the plastic deformation of the adherends. The thick metal joint results show close agreement with the finite element results. The Thouless model produced a higher value, but it should also be noted that there was

CASE 1	Crack Length	2.420 in
	Deflection	0.605 in
	Total Strain Energy	6.85 lbin
	Plastic Dissipation	2.22 lbin
	Recoverable Energy	4.63 lbin
CASE 2	Crack Length	2.433 in
	Deflection	0.620 in
	Total Strain Energy	7.05 lbin
	Plastic Dissipation	2.35 lbin
	Recoverable Energy	4.69 lbin
CASE 3	Crack Length	2.444 in
	Deflection	0.636 in
	Total Strain Energy	7.27 lbin
	Plastic Dissipation	2.50 lbin
	Recoverable Energy	4.76 lbin
CASE 4	Crack Length	2.452 in
	Deflection	0.646 in
	Total Strain Energy	7.41 lbin
	Plastic Dissipation	2.60 lbin
	Recoverable Energy	4.81 lbin
CASE 5	Crack Length	2.461 in
	Deflection	0.659 in
	Total Strain Energy	7.60 lbin
	Plastic Dissipation	2.73 lbin
	Recoverable Energy	4.87 lbin

Table 5.3: FE model results – deflection and energy values

Method	G_c (lb/in)
Experimental, thin metal	10.52
Experimental, thick metal	4.83
Thouless Model, thin metal	7.45
FE Plastic Model, thin metal	4.18

Table 5.4: Comparison of G_c results from different methods using primed metal/metal DCB joints

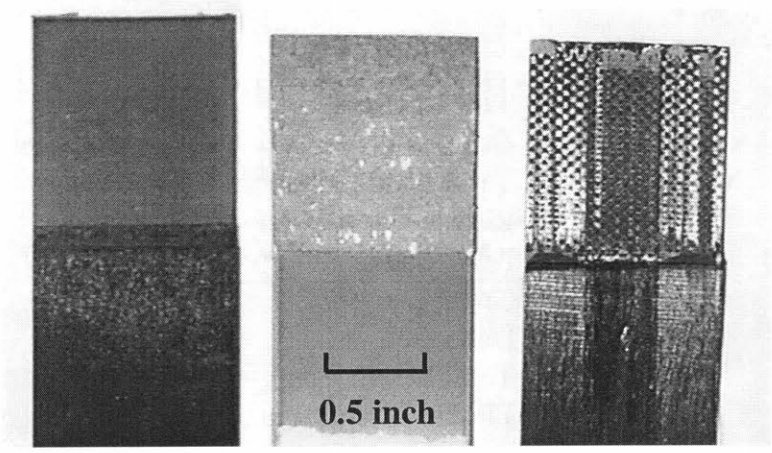

Figure 5-7: Examples of the three types of failure modes

a high degree of scatter in the data reduced by this method and it is probably not as reliable as the other methods. Overall, it seems as though the plastic deformation of the joints over-predicted the critical strain energy release rate by a factor of two.

5.3 Failure Modes

As described in Section 4.2, three different failure modes were observed experimentally. Figure 5-7 shows examples of each of these types. On the left is an as-cured composite adherend displaying adhesive failure. The middle picture is a primed metal adherend from a metal/metal joint showing cohesive failure. On the right is a co-cured composite adherend showing adherend failure, because of the extensive damage done to the composite fibers.

Cohesive failure was observed in the homogeneous specimens and in some of the secondarily cured specimens. Adhesive failure was only observed in specimens where the surfaces were prepared inadequately; the as-cured and peel-ply composite surfaces are examples of this. The third type of failure was adherend failure. In this study, two variants of this failure mode were observed. The first was when the grooved metal DLS specimens broke in half perpendicular to the loading direction, fracturing the metal doublers but not breaking in the adhesive. The second, more common occurance was when the crack propagated within the composite adherend. This happened in

approximately 70% of the DCB specimens, where composite plies often delaminated. It was also common on the co-cured DLS specimens where the composite adherends sustained significant fiber breakage.

Table 5.5 summarizes the failure mechanisms for each of the specimen types tested. As shown in the chart, most of the DCB specimens failed within the composite. In these cases, a layer of fibers was left adhering to the metal surface. The homogeneous specimens in general failed cohesively. The homogeneous DCB specimens also failed progressively, whereas most of the composite/metal bonds failed catastrophically, often breaking several millimeters at a time. This is due to the thermal residual stresses locked inside the metal/composite bonds due to the thermal expansion mismatch.

The difference between catastrophic and progressive failure in the DCB specimens can also be seen graphically by looking at the load-displacement curves produced from the test data. Figures 5-8 and 5-9 show such curves for the two types of homogeneous specimens, which display progressive crack growth. Figures 5-10 and 5-11 show such curves for grooved and primed/sanded specimens, which display catastrophic crack growth. Here, one can see the difference between the grooved specimens, for example, and the all-composite specimens. The grooved specimen shows a sharp decrease in load corresponding to crack initiation. In contrast, the composite specimen shows a smoother curve, with smaller dips marking crack growth. Catastrophic failure, not seen in the homogeneous specimens, is due to the thermal residual stresses that are locked into the composite/metal joints because of the CTE mismatch.

5.4 Stiffness and Thermal Imbalances

As described in Section 2.3, joints that have mismatched elastic and thermal properties will have reduced strength properties. Hart-Smith [14, 15] derived formulas quantifying the amount of strength reduction in double lap shear joints due to mismatched adherends. While a balanced joint will symmetrically deform the adhesive, an unbalanced one will cause the adhesive to be loaded more heavily on one end, thus causing premature failure. Equations 2.4 and 2.5 predict the reduction in strength due

Composite/Metal	Type	Failure Mode
Sanded/Primed	DLS	Mostly cohesive, some fibers stuck to metal
	DCB	Cohesive turns to composite delamination
Sanded/Anodized	DLS	Cohesive, metal surface, and composite failure mix
	DCB	Cohesive turns to composite delamination
Sanded/Sanded	DLS	Mostly cohesive, some fibers stuck to metal
	DCB	Mostly composite delamination, some fibers stuck to metal
Co-Cured/Primed	DLS	Composite failure
	DCB	Progressive; Mostly composite delamination
Postcured/Primed	DLS	Composite failure
	DCB	Mostly composite delamination
Unsanded/Sanded	DLS	Adhesive failure at composite surface
	DCB	Adhesive failure at composite surface
Sanded/Primed	DLS	Some fibers stuck to metal
(FM-300)	DCB	Composite delamination
Co-Cured/Grooved	DLS	Metal fractured, some fibers stuck to metal
	DCB	Mostly composite delamination
Peel-Ply/Sanded	DLS	Adhesive failure at composite surface
	DCB	N/A
Quasi-isotropic/Primed	DLS	Composite delamination failure–thermal
(Cocured)	DCB	Composite delamination failure–thermal
Sanded/Primed	DLS	Mostly cohesive; adhesive at defect locations
(Defects)	DCB	Composite delamination
All Metal	DLS	Cohesive
(Sanded)	DCB	Progressive; Cohesive
All Metal	DLS	Cohesive
(Primed)	DCB	Progressive; Cohesive
All Composite	DLS	Mostly cohesive, some fiber breakage
(Sanded)	DCB	Progressive; Some cohesive, some fiber failure

Table 5.5: Failure modes for each specimen type

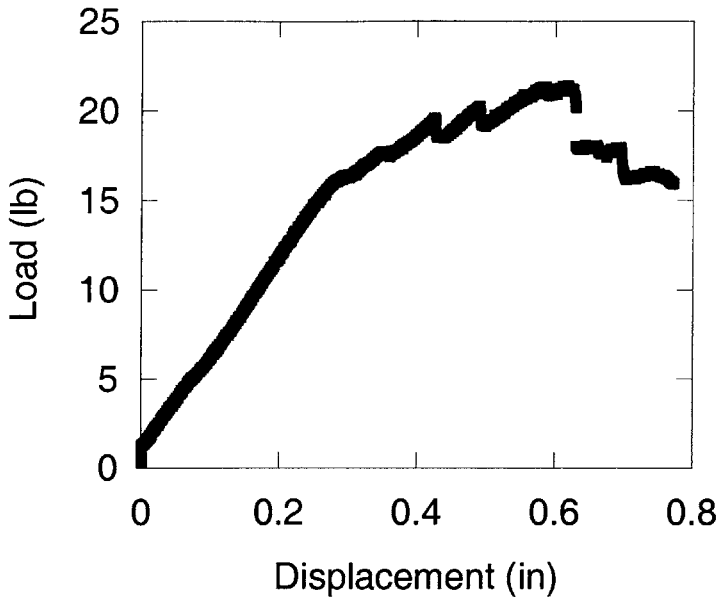

Figure 5-8: Load-displacement plot of composite-composite DCB specimen displaying progressive failure

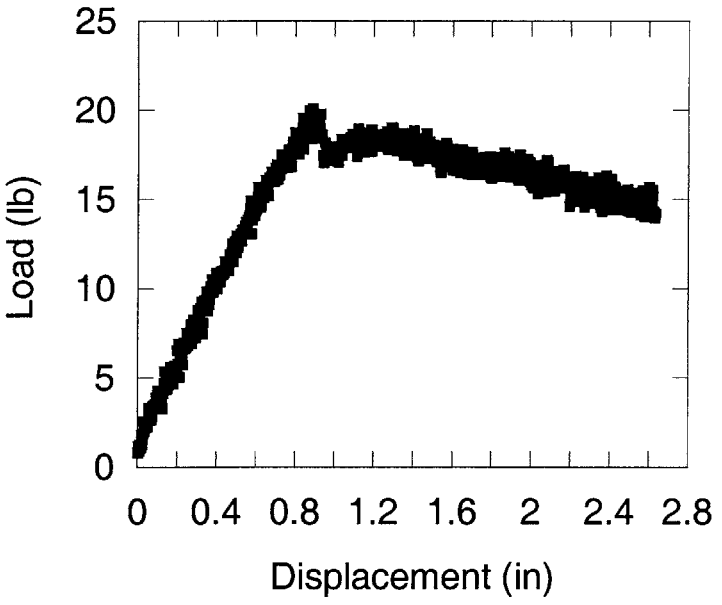

Figure 5-9: Load-displacement plot of primed metal/metal DCB specimen displaying progressive failure

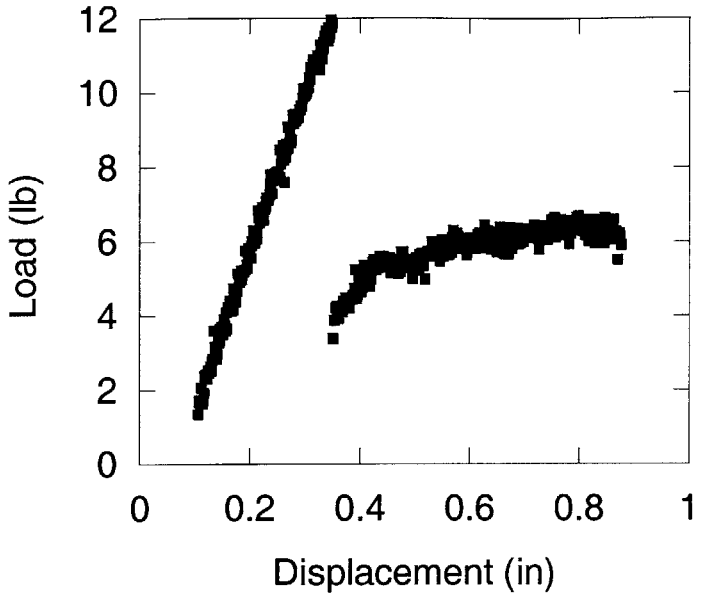

Figure 5-10: Load-displacement plot of grooved/co-cured DCB specimen displaying catastrophic failure

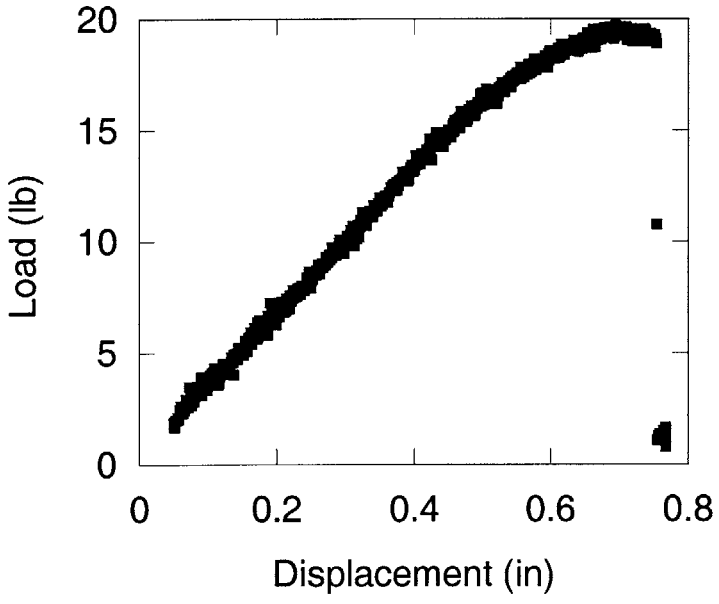

Figure 5-11: Load-displacement plot of primed/sanded DCB specimen displaying catastrophic failure

to adherend stiffness mismatch by taking into account the elastic moduli and thicknesses of the three adherends (two of which are identical). Using these equations with the specimen configuration and materials from this study,

$$S = \frac{E_i t_i}{2E_o t_o} = 1.31 \tag{5.4}$$

for a unidirectional composite laminate as the inner adherend. Note that a perfectly stiffness-balanced joint would have a value of $S = 1$. This imbalance results in a stiffness reduction factor of

$$\sqrt{\frac{1 + \frac{1}{S}}{2}} = 0.94 \tag{5.5}$$

meaning that because of the adherend stiffness imbalance, only 94% of the potential theoretical bond strength is predicted. The bond becomes inefficient because one end of the adhesive is straining more than the other, and thus breaks first. Note that these equations only take into account the stiffness imbalance; no thermal mismatch effect is accounted for here.

Hart-Smith [14, 15] also provides a formula for the reduction of strength due to thermal mismatches by taking into account the residual stresses locked in the joint during the cure cycle. For a stiffness-balanced joint, using the properties of the joints in this study, this results in

$$ThermalReduction = 2E_o t_o \Delta\alpha\Delta T = -4730 lb/in \tag{5.6}$$

for a co-cured joint experiencing a temperature change of -280°F. However, this does not accurately reflect the strength reduction in the joints in this study because the joints are *not* stiffness-balanced.

To solve this problem, Hart-Smith also provides Equations 2.9 to predict the maximum load carrying capabilities of joints that have both thermal and stiffness imbalances. For these equations, the specific material properties of the adhesive, as diagrammed in Figure 2-9, are needed. The properties for FM-300^{TM}were idealized from shear stress/strain data provided by Cytec, and have the values τ_p=7210psi,

γ_e=1.4, and γ_p=0.40. This results in the parameter $\eta\tau_p(\frac{1}{2}\gamma_e + \gamma_p)$=23.7 lb/in. Substituting this into the strength equations, the two values are P=13,195 lb/in and P=19,558 lb/in. This suggests that the theoretical strength of the joint, taking stiffness and thermal imbalances into account, is 13,195 lb/in for a co-cured, unidirectional composite/metal joint as used in this study. Needless to say, this is *much* higher than the strengths measured experimentally for *any* specimen surface preparation. This is probably due to inaccuracies in the idealized adhesive model as well as experimental inefficiencies due to imperfect specimen manufacturing.

5.5 Thermal Effects

Bonding together two thermally dissimilar materials at high temperatures causes thermal residual stresses to form within the joints. This can cause premature fractures and delaminations immediately after curing, or catastrophic failures in DCB joints during testing. In this study, two measures of the effects of temperature on bonding metal/composite joints were used. First, the influence of the CTE of the composite adherends was measured by manufacturing specimens with different lay-ups. Secondly, an analysis used by Shetty[16, 31] was employed to compare secondarily-cured and co-cured DCB results. These two methods are described in the following sections.

5.5.1 Composite Lay-Up Effects

The extent of thermal mismatch between aluminum and different composite layups can be determined by comparing the induced thermal stresses. These can be calculated using the modulus, CTE, and temperature change of the material. In this case, all the materials underwent the same temperature change due to curing, so this can be omitted for comparison purposes. An equivalent modulus, or stiffness, can be calculated for any composite laminate using Classical Laminated Plate Theory. The laminate CTEs can also be calculated with this method.

Laminate	CTE ($\mu m/m°C$)	$E_{comp}(GPa)$	$\Gamma\left(GPa\left(\frac{\mu m}{m°C}\right)^2\right)$
$[0_{16}]$	0.02	148.9	80.7
$[0_2/\pm 30_2/0_2]_s$	2.83	119.3	50.0
$[0_2/\pm 30/\pm 60/0_2]_s$	5.64	102.0	31.8
$[0_2/\pm 45_2/0_2]_s$	5.64	97.9	30.5
$[0_2/\pm 30/\pm 60/90_2]_s$	11.26	67.3	9.8
$[0_2/\pm 45_2/90_2]_s$	11.26	63.2	9.2

Table 5.6: Thermal mismatch parameter values

The mismatch is compared using the parameter

$$\Gamma = E_{comp}(\alpha_{comp} - \alpha_{alum})^2 \tag{5.7}$$

where E_{comp} is the Young's modulus of the composite laminate, and α_{comp} and α_{alum} are the CTEs of the composite and aluminum, respectively. Table 5.6 shows numerical results for several different laminates. From this chart, one can see that the unidirectional laminate has the highest thermal mismatch. The quasi-isotropic has the lowest, and therefore should have the lowest residual stresses in the metal-composite joint.

However, it was found experimentally that the quasi-isotropic laminate delaminated after co-curing with the aluminum (see Section 4.12). This was because a new damage mode was introduced. The interlaminar strength between the internal composite plies was not high enough to resist delamination due to the stresses induced by the thermal loads on the specimens. While changing the composite lay-up from unidirectional to quasi-isotropic reduces the thermal mismatch and thus reduces the in-plane thermal stresses, it also increased the interlaminar stress between the composite plies.

5.5.2 Manufacturing Effects on DCB Specimens

Experimentally, it was found that in general the co-cured DCB joints had lower toughnesses than the secondarily cured joints. This could be due in part to the fact that the co-cured joints were exposed to a larger temperature drop during curing

than the secondarily cured specimens. Shetty [16, 31] performed analyses predicting the strain energy release rate in double cantilever metal/composite joints due solely to *thermal* loads, such as those experienced during the cure cycle. The strain energy release rate is defined as

$$G = \frac{{\epsilon_t}^2 t_1 E_1}{2+\lambda\xi} - \frac{\beta^2 t_1 \left(\lambda\xi^3+1\right)}{2E_1}\left[\xi^2\left(\lambda\xi+1\right)\left(\lambda\xi^3+1\right)+3\lambda\xi^3\left(\xi+1\right)^2\right] \tag{5.8}$$

where $\xi = \frac{t_1}{t_2}$ is the ratio of the adherend thicknesses, $\lambda = \frac{E_1}{E_2}$ is the ratio of the elastic moduli, $\epsilon_t = (\alpha_1 - \alpha_2)\,\Delta T$ is the free thermal strain, and $\beta = \frac{\epsilon_t E_1}{\xi(\lambda\xi^3+1)(\lambda\xi+1)+3\lambda\xi^2(\xi+1)^2}$. In this model, the outer (metal) adherends are described by t_2 and E_2 and the inner (composite) adherend properties are denoted with the subscript "1".

Using the material properties and geometries studied in this work, the strain energy release rate due to the temperature drop experienced during a 350°F co-cure is 3.854 lb/in. For a secondary cure at 225°, the strain energy release rate is 1.181 lb/in. If these values are then added on to the corresponding experimentally measured *mechanical* strain energy release rates, the total strain energy release rates can be compared. Strain energy release rates cannot be directly added, but because they are proportional to the square of the stress intensity factors, for which superposition applies, the following holds true:

$$G_{total} \propto \left(\sqrt{G_{thermal}} + \sqrt{G_{mechanical}}\right)^2 \tag{5.9}$$

In this way, a more accurate representation of the effects of surface preparation can be made.

Figure 5-12 compares the mechanical strain energy release rates discussed earlier with the thermo-mechanical strain energy release rate values calculated from the above equations. These results show that the thermal loads have a significant effect on the total strain energy release rate. In fact, in some cases the thermal contribution is greater than the mechanical contribution to G_{total}. A difference can still be seen between the different surface preparation methods, however. Most notable is that the grooved specimens show one of the highest fracture toughnesses when the thermal

effects are taken into account. This could mean that the patterning procedure has a more beneficial effect on fracture-critical (DCB) structures than on strength-critical (DLS) structures.

5.6 Patterning

Unfortunately, it seems that by etching grooves in the metal and therefore removing material, the aluminum was significantly weaker than a similar, un-etched piece of aluminum. The grooves gave the metal doublers in the DLS specimens a smaller cross-sectional area, and therefore the metal could not withstand as high stress levels as the un-etched metal. Furthermore, the grooves could have introduced stress concentrations into the metal, causing it to fail at lower loads than the plain metal. Patterning the metal is perhaps not a viable solution for increasing bond strength because in this case, it is possible to have the metal itself fail before the adhesive.

These results could potentially be improved, however. Making the aluminum adherends slightly thicker may alleviate the early metal failure problem. It is also possible that grooves are not the optimal pattern for this application. The grooves in this study did not penetrate the composite plies. Sharp spikes that are allowed to penetrate the composite adherends may better simulate the "stitching" effect and provide more through thickness reinforcement. The DCB specimens in particular did not exhibit much of a strengthening effect due to the grooves because the specimens nearly always failed within the composite adherends and not within the adhesive. Therefore, any crack stopping potential the grooves may have had could not be realized.

5.7 Summary

Several issues that arose during the experimental part of this study were discussed here. It was concluded that the primed metal/metal DCB tests produced unrealistically high values for the critical strain energy release rate due to the plastic defor-

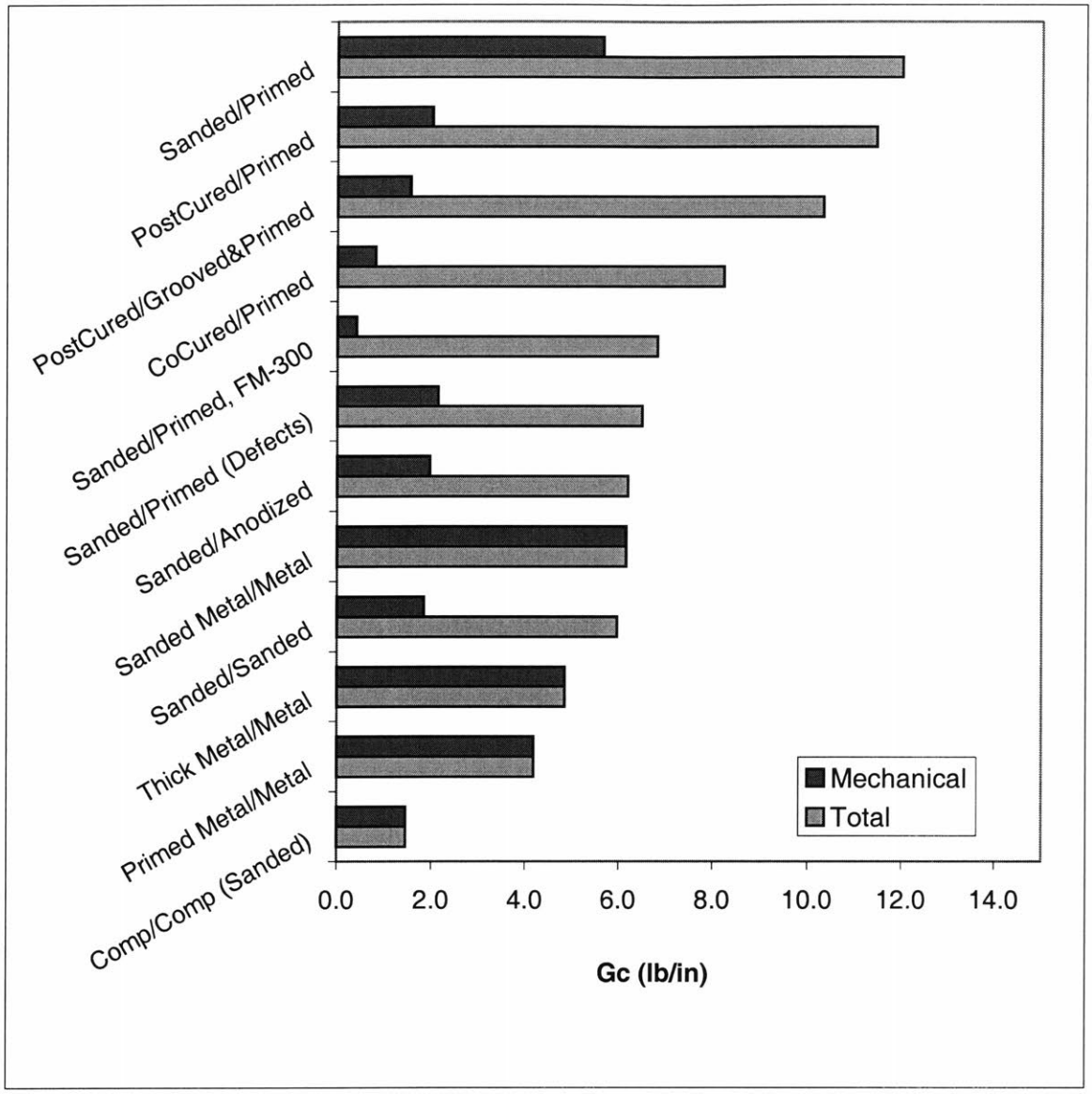

Figure 5-12: Comparison of total and mechanical strain energy release rates

mation of the adherends. Experiments using thicker metal that would not yield and finite element analyses showed that a more realistic value for G_c is less than half that of the original specimens.

The failure modes of the specimens varied with surface preparation. Poor surface preparations such as unsanded composite surfaces cause adhesive failure because the adhesive did not adhere to the surface. Cohesive failure within the adhesive itself was observed in many of the homogeneous specimens and some of the secondarily cured specimens. Adherend failure was common in the form of composite delamination, especially in the DCB specimens. The DCB specimens themselves also exhibited either catastrophic or progressive failure, due to the presence or lack of thermal residual stresses in the joint.

The effects of bonding together two different materials with different properties was twofold. First, the stiffness mismatch caused a reduction in strength in the DLS joints, as explained by Hart-Smith's analysis. More importantly, the coefficient of thermal expansion mismatch between the two materials had a significant effect on both specimen configurations, but was especially realized in the DCB specimens. In some cases, the thermal residual stresses caused by the CTE mismatch were enough to crack the specimens without any applied mechanical load. In others, the thermal strain energy release rate was shown to be a significant portion of the total strain energy release rate.

Patterning the metal was shown to have adverse effects on the DLS specimens because the metal adherends were weakened by the patterning process, and this caused the specimens to fail prematurely. When thermal effects were taken into account, the grooved DCB specimens proved to have relatively high fracture toughnesses, however. This may indicate that the patterning process has potential for use as a bond strengthening agent.

The next chapter will highlight the conclusions drawn from the experimental and analytical studies performed in this work.

Chapter 6

Conclusions

Several conclusions can be drawn from this work. Most importantly, it has been shown that a good surface preparation is necessary for the production of a high strength, high reliability bond. Patterning the specimens did not seem to improve DLS bond strength, but showed some potential in improving the fracture toughness of the joints. The manufacturing method used, either secondary curing or co-curing, also has an effect on failure mode and bond strength, mainly due to the difference in cure temperature. The failure mechanisms of the specimens varied with surface preparation and manufacturing method as well. Care needs to be taken in analyzing test results where plasticity is involved because plastically deforming adherends cause inaccurate measurements of the strain energy release rate in DCB specimens. Finally, thermal residual stresses in the bonds caused some premature bond failures, and the strain energy release rates due to the thermal loads were a significant fraction of the total strain energy release rates of the metal/composite joints. The following sections will describe each of these aspects in more detail.

The thesis will then conclude with recommendations for future work.

6.1 Surface Preparation Effects

From the test results, it is obvious that the way the surfaces of jointed materials are prepared is crucial to the strength of the bond. In this work, numerous surface

preparation methods were explored, and the results differed widely. The best results were obtained when the metal surfaces were primed with BR-127 primer and the composite surfaces were abraded with sandpaper.

Putting grooves in the metal surface did not noticeably improve the characteristics of the joint. The grooved DCB specimens performed similarly to the co-cured specimens, and had one of the highest strain energy release rate values when thermal effects were taken into account. The DLS results were encouraging because the adhesive bond strengths were only limited by the metal adherends. However, if the etching process weakens the adherends, as seems to be the case, this is not a good solution to improving bond strength and reliability.

6.2 Manufacturing Method Effects

There was also a significant difference in both bond strength and toughness depending on whether the specimens were co-cured or secondarily cured. Co-cured specimens tended to fail at a lower load than the secondarily cured specimens. Most of the effect is presumed to be due to the higher cure temperature, since the published values of shear strength for FM-300 and FM-123-2 differ by a negligible amount. Sanded composite/primed metal DLS results using both FM-123 at a low cure temperature and FM-300 at a higher cure temperature showed that the higher cure temperature specimens broke at half the failure load of the lower cure temperature ones. This is much too great of a difference to be accounted for only by the difference in adhesive strength.

6.3 Failure Mechanisms

Three different failure modes were observed in the mechanically tested specimens. Cohesive failure was seen in all the homogeneous tests, as well as in most of the secondarily-cured specimens. Adhesive failure was seen only in specimens where the secondarily-cured composite surfaces were not sanded. As-cured and peel-ply surfaces

were not adequate preparations for the FM-123 adhesive to adhere. Adherend failure was found in two forms: metal failure in the grooved specimens, and composite failure in many of the co-cured specimens and most of the DCB specimens.

The DCB specimens themselves showed two different types of failure: progressive and catastrophic. Only the homogeneous specimens showed true progressive failure. The metal/composite specimens, because of the thermal residual stresses, failed catastrophically, with crack advances of a centimeter or more all occurring in an unstable manner.

6.4 Plasticity Effects

Plastic deformation of the metal adherends was observed in the metal/metal and primed/sanded DCB joints. This resulted in abnormally high calculated values of the critical strain energy release rate. Experimental, analytical, and numerical methods were used to obtain a better understanding of this effect. The thick metal adherend joints and the FE analysis gave similar results, and showed that the plasticity in the original primed metal joints caused G_c to be over-predicted by a factor of two.

6.5 Thermal Effects

The thermal mismatch between the metal and composite adherends significantly affected the strength and toughness of the joints studied in this work. In some cases, the thermal residual stresses were enough to fracture the specimens without the application of any mechanical load. The strain energy release rates due to the induced thermal loads were quite significant, and comprised a large fraction of the total strain energy release rate in the co-cured specimens.

6.6 Summary

In summary, a process for manufacturing high quality metal/composite joints has been established. Overall, the best results are obtained when secondarily cured joints are made with sanded composite surfaces and primed metal surfaces. Care should be taken when analyzing these joints due to the effects of thermal loads and plastically deforming adherends.

6.7 Recommendations for Future Work

More studies need to be performed on joints with patterned metal surfaces. The potential for increased bond toughness was observed here, but a solution to the low metal strength in the DLS specimens needs to be found. Thicker metal adherends may help, although care should be taken such that the increased thermal stresses due to the thicker adherends do not cause bond failure. Performing tests using patterns other than grooves may also prove beneficial. Specifically, allowing the surface patterns to penetrate the composite surface may produce dramatically different results.

Another area of interest is the effects of the environment on metal/composite adhesive joints. Adhesive joints on an aircraft are not kept in carefully controlled surroundings, but are instead exposed to moisture and heat. The durability of metal composite bonds under high temperatures and humid environments needs to be investigated. The surface preparation methods recommended from the testing performed in this study may not show the same results under these extreme conditions.

The fatigue properties of these joints also need to be studied. Typical aircraft perform thousands of flights during their lifetimes, and the characteristic mechanical loads associated with in-flight maneuvers, take-offs, and landings all degrade the structure over time. Cyclic thermal loads and thermo-mechanical fatigue loading is also experienced during flight, and an understanding of these effects is therefore crucial to producing reliable joints. Patterned surfaces or other surface preparation methods may prove to be more beneficial under these conditions.

Finally, an overall approach to the design of structural metal/composite adhesive joints needs to be developed. Applying the flat test coupon results to an actual, full-sized aircraft structure or WASP structure could prove difficult. These structures may also need to be manufactured using different methods, and this could affect the reliability of the joints. Tests on more representative joint geometries therefore need to be performed. Once again, surface preparation and manufacturing methods that were shown to produce quality coupons may not be adequate for differently-shaped and possibly larger components.

If metal/composite adhesive bonds are to be used more widely in aircraft structures, it is crucial that these issues be addressed. Continued work on patterned joints, as well as studies to characterize the effects of extreme environmental conditions, thermal and mechanical fatigue loading, and shape and scale are essential. With a better understanding of these effects, the advantages of having adhesively bonded metal/composite joints in aircraft structures will be realized.

Bibliography

[1] Higgins, A., "Adhesive Bonding of Aircraft Structures," *International Journal of Adhesion and Adhesives*, Vol. 20, 2000, pp. 367–376.

[2] Tsai, S., *Theory of Composites Design*, Think Composites, 1992.

[3] Andrews, D., ed., *Soldering, Brazing, Welding, and Adhesives*, The Institution of Production Engineers, 1978.

[4] Hart-Smith, L., "An Engineer's Viewpoint on Design and Analysis of Aircraft Structural Joints," *Proceedings of the Institute of Mechanical Engineers, Part G: Journal of Aerospace Engineering*, Vol. 209, 1995, pp. 105–129.

[5] Hoskin, B. and A. Baker, eds., *Composite Materials for Aircraft Structures*, AIAA Education Series, American Institute of Aeronautics and Astronautics, Inc., 1986.

[6] Sawyer, J., "Effect of Stitching on the Strength of Bonded Composite Single Lap Joints," *AIAA Journal*, Vol. 23, No. 11, 1985, pp. 1744–1748.

[7] Davis, M. and D. Bond, "Principles and Practices of Adhesive Bonded Structural Joints and Repairs," *International Journal of Adhesion and Adhesives*, Vol. 19, 1999, pp. 91–105.

[8] DeVries, K. and G. Anderson, "Analysis and Design of Adhesive-Bonded Joint," in *Bonded Joints and Preparation for Bonding*, No. AGARD-LS-102, Advisory Group for Aerospace Research and Development, 1979, pp. 3–1–3–25.

[9] ASTM, "Standard Test Method for Apparent Shear Strength of Single-Lap-Joint Adhesively Bonded Metal Specimens by Tension Loading (Metal-to-Metal)," in *Book of ASTM Standards.*

[10] ASTM, "Standard Test Method for Strength Properties of Double Lap Shear Adhesive Joints by Tension Loading," in *Book of ASTM Standards.*

[11] ASTM, "Standard Guide for Use of Adhesive-Bonded Single Lap-Joint Specimen Test Results," in *Book of ASTM Standards.*

[12] ASTM, "Standard Test Method for Mode I Interlaminar Fracture Toughness of Unidirectional Fiber-Reinforced Polymer Matrix Composites," in *Book of ASTM Standards.*

[13] ASTM, "Standard Test Method for Fracture Strength in Cleavage of Adhesives in Bonded Metal Joints," in *Book of ASTM Standards.*

[14] Hart-Smith, L., "Analysis and Design of Advanced Composite Bonded Joints," Tech. Rep. CR-2218, NASA, 1974.

[15] Hart-Smith, L., "Adhesive-Bonded Double-Lap Joints," Tech. Rep. CR-112235, NASA, 1973.

[16] Shetty, S. and S. M. Spearing, "The Reliability of Composite-Metal Adhesive Joints Subject to Thermo-Mechanical Loading," *AIAA Journal*, Vol. AIAA-97-1222, 1997, pp. 1080–1087.

[17] Loftus, D., M. Found, and J. Yates, "The Performance of Aluminum to Carbon Fibre Composite Bonded Joints in Motorsport Applications," *Sports Engineering*, Vol. 2, 1999, pp. 235–243.

[18] ASTM, "Standard Guide for Preparation of Metal Surfaces for Adhesive Bonding," in *Book of ASTM Standards.*

[19] McMillan, J., "Surface Preparation–The Key to Bondment Durability," in *Bonded Joints and Preparation for Bonding*, No. AGARD-LS-102, Advisory Group for Aerospace Research and Development, 1979, pp. 7–1–7–30.

[20] Keohan, F., A. Mitchell, C. Ragan, and L. Bialic, "A New Chromium-Free Surface Treatment for Structural Adhesive Bonding of Aluminum," in *38th International SAMPE Symposium*, 1993, pp. 1181–1195.

[21] Blohowiak, K., J. Osborne, K. Krienke, and D. Sekits, "Sol-Gel Surface Treatments for Adhesive Bonding of Titanium and Aluminum Structures," in *28th International SAMPE Technical Conference*, 1996, pp. 440–470.

[22] Koch, G., G. Todd, and A. Deutchman, "Non-Chemical Surface Treatment for Adhesive Bonding of Aircraft Aluminum Alloys," in *Technology Transfer in a Global Community International SAMPE Technical Conference*, Vol. 28, (Covina, CA), SAMPE, 1996, pp. 457–463.

[23] Chin, J. and J. Wightman, "Surface Pretreatment and Adhesive Bonding of Carbon Fiber-Reinforced Epoxy Composites," in *Composites Bonding, ASTM STP 1227*, pp. 1–16, American Society of Testing and Materials, 1994.

[24] Marinelli, J. and C. Lambing, "A Study of Surface Treatments for Adhesive Bonding of Composite Materials," in *38th International SAMPE Symposium*, 1993, pp. 1196–1209.

[25] Glaessgen, E., I. Raju, and C. J. Poe, "Delamination and Stitch Failure in Stitched Composite Joints," *AIAA Journal*, Vol. AIAA-99-1247, 1999.

[26] Freitas, G. and M. Dubberly, "Joining Aluminum Materials Using Ultrasonic Impactors," *Journal of Materials*, May 1997, pp. 31–32.

[27] Allen, D., *The Principles and Practice of Photochemical Machining and Photoetching*, Adam Hilger, 1986.

[28] Lagace, P., M. Beaumont, J. Brewer, and C. Varnerin, "TELAC Manufacturing Course Class Notes," tech. rep., Technology Laboratory for Advanced Composites, MIT, 1991.

[29] Crandall, S., N. Dahl, and T. Lardner, eds., *An Introduction to the Mechanics of Solids*, Crandall, S., N. Dahl, and T. Lardner, eds., McGraw-Hill, Inc., 1978.

[30] Hart-Smith, L., G. Redmond, and M. Davis, "The Curse of the Nylon Peel Ply," in *41st International SAMPE Symposium*, SAMPE, 1996, pp. 303–317.

[31] Shetty, S. P., *Fracture and Failure of Layered Materials Under Thermo-Mechanical Loading*, Master's thesis, Massachusetts Institute of Technology, 1997.

[32] Thouless, M., J. Adams, M. Kafkalidid, S. Ward, R. Dickie, and W. G.L., "Determining the Toughness of Plastically Deforming Joints," *Journal of Materials Science*, Vol. 33, 1998, pp. 189–197.

[33] Thouless, M., M. Kafkalidis, S. Ward, and Y. Bankowski, "Toughness of Plastically-Deforming Asymmetric Joints," *Scripta Materialia*, Vol. 37, No. 7, 1997, pp. 1081–1087.

[34] Yang, Q., M. Thouless, and S. Ward, "Numerical Simulations of Adhesively-Bonded Beams Failing with Extensive Plastic Deformation," *Journal of the Mechanics and Physics of Solids*, Vol. 47, 1999, pp. 1337–1353.

[35] ASTM, "Standard Test Method for Tensile Strain-Hardening Exponents (n-values) of Metallic Sheet Materials," in *Book of ASTM Standards.*